# Source apportionment and ecotoxicity of PM2.5 pollution events in a Major Southern Hemisphere Megacity: influence of a biofuel impacted fleet and biomass burning

Guilherme Martins Pereira[1,2], Leonardo Yoshiaki Kamigauti[1], Rubens Fabio Pereira[1], Djacinto Monteiro dos Santos[3], Thayná da Silva Santos[2], José Vinicius Martins[4], Célia Alves[5], Cátia Gonçalves[5,a], Ismael Casotti Rienda[5], Nora Kováts[6], Thiago Nogueira[7], Luciana Rizzo[3], Paulo Artaxo[3], Regina Maura de Miranda[8], Marcia Akemi Yamasoe[1], Edmilson Dias de Freitas[1], Pérola de Castro Vasconcellos[2], Maria de Fatima Andrade[1]

[1]Department of Atmospheric Sciences, Institute of Astronomy, Geophysics and Atmospheric Sciences, University of São Paulo, 05508-090, São Paulo, Brazil.

[2]Department of Chemistry, Institute of Chemistry, University of São Paulo, 05508-000, São Paulo, Brazil.

[3]Department of Applied Physics, Institute of Physics, University of São Paulo, 05508-090, São Paulo, Brazil.

[4]Department of Mineralogy and Geotectonics, Institute of Geosciences, University of São Paulo, 05508-080, São Paulo, Brazil.

[5]Center for Environmental and Marine Studies, Department of Environment and Planning, University of Aveiro, 3810-193 Aveiro, Portugal

[6]Center of Natural Environmental Sciences, University of Pannonia, Egyetem str. 10, 8200 Veszprém, Hungary

[7]Department of Environmental Health, School of Public Health, University of São Paulo, 01246-904, São Paulo, Brazil.

[8]School of Arts, Sciences and Humanities, University of São Paulo, 03828-000, São Paulo, Brazil.

[a]Current address: Department of Physics, University of León, Campus de Vegazana, 24071 León, Spain.

*Correspondence to:* Guilherme Martins Pereira (guilherme.martins.pereira@usp.br)

**Abstract.** The Metropolitan Area of São Paulo (MASP) in Brazil has reduced its vehicular emissions in the last decades. However, it is still affected by air pollution events, mainly in the winter, characterized as a dry season. The chemical composition of fine particulate matter (PM2.5) was studied in the MASP during a 100-day dry period in 2019. PM2.5 samples underwent an extensive chemical characterization (including inorganic and organic species), and submicrometer particle number size distributions were simultaneously monitored. PM2.5 concentrations exceeded the new World Health Organization's daily guidelines on 75% of sampling days, emphasizing the need for strengthening local regulations. Source apportionment (Positive Matrix Factorization, PMF5.0) was performed, and the sources related to vehicular emissions remain relevant (over 40% of PM2.5). A high contribution of biomass burning was observed, reaching 25% of PM2.5 mass and correlated with sample ecotoxicity. This input was associated with north and northwest winds, suggesting other emerging sources besides sugarcane burning (forest fires and sugarcane bagasse power plants). A mixed factor of road dust and vehicular emissions increased throughout the campaign was related to stronger winds, suggesting a significant resuspension. The sulfate secondary formation was related to humid conditions. Additionally, monitoring size particle distribution allowed the observation of particle growth on days impacted by secondary formation. The results pointed out that control measures of high

34  PM$_{2.5}$ events should include the control of emerging biomass burning sources in addition to stricter rules concerning vehicular

35  emissions.

## 1       Introduction

37  According to the World Health Organization (WHO), a large part of the world's population lives in places where the

38  recommended air quality standards are not achieved, and this includes the Metropolitan Area of São Paulo (MASP), Brazil

39  (WHO, 2021; CETESB 2023). In the MASP, thousands of tons of pollutants are released into the atmosphere every year. The

40  MASP has more than 21 million inhabitants and around 7 million vehicles. In 2022, in the MASP, vehicles were responsible

41  for 96% of CO emissions, 70% of HC, 60% of NO$_x$, 8% of SO$_2$, and 37% of fine-mode particulate matter (PM$_{2.5}$) (CETESB,

42  2023). Among the pollutants, particulate matter is extensively studied, as it harms human health and is associated with

43  cardiovascular diseases and cancer (Cohen et al., 2017). Furthermore, particulate matter has direct climatic effects through the

44  absorption and scattering of solar radiation and indirect by affecting cloud microphysics (Li et al., 2022; Pöschl, 2005).

45  The fine fraction of particulate matter (PM$_{2.5}$) comprises particles with aerodynamic diameters equal to or below 2.5

46  μm that can penetrate the respiratory system, reaching the alveoli. Smaller particles than 100 nm are called ultrafine particles

47  and can reach other organs through the lung vasculature (Schraufnagel, 2020; Kumar et al., 2014). Particles are emitted by

48  different natural sources, such as volcanic eruptions, resuspension, and erosion of soils and vegetation, while the dominant

49  anthropogenic sources are vehicles, industrial activities, and biomass burning. The formation of secondary particles is quite

50  significant in some cities, such as São Paulo, where sulfate and nitrate concentrations are high and secondary particles can

51  comprise half of PM$_{2.5}$ mass (Andrade et al., 2012; CETESB et al., 2023). Particulate matter is a complex mixture, including

52  inorganic species (water-soluble ions and element oxides) and carbonaceous species, such as elemental carbon (EC, associated

53  with soot) and organic carbon (OC) associated with organic compounds. Some particulate organic species present toxic

54  properties, such as polycyclic aromatic hydrocarbons (PAHs) (Ravindra et al., 2008; Pöschl, 2005).

55  The vehicle fuel profile in the MASP is unique compared to other metropolises worldwide, with a significant proportion

56  of biofuels, especially in light-duty vehicles (LDVs) (Andrade et al., 2017). The fleet has been running in gasoline and

57  bioethanol blends (gasohol, 73% of gasoline, 27%, ethanol), hydrated ethanol (5% of water), diesel and biodiesel blends (9%

58  of biodiesel produced from soybean) (Pereira et al., 2023a,b). The highest levels of ethanol usage were achieved by late 2018,

59  reaching levels comparable to those of gasohol (Pereira et al., 2023a). Although the vehicle fleet has significantly increased

60  since the 1980's, particulate pollutants have decreased over the past few decades (Andrade et al., 2017). Furthermore, a rise in

61  the relative contribution of non-exhaust sources is expected in the next years due to control measures focused on vehicle

62  exhaust (Thorpe and Harrison, 2008). A recent source apportionment study conducted in a densely populated area of the

63  MASP, which experiences heavy vehicle traffic and has numerous industries, found that in 2019, light-duty vehicles

64  contributed to 9.9% of PM, while heavy-duty vehicles (HDVs) accounted for 42% (Vieira et al., 2023). Sugarcane biomass

65  burning typically influences air quality in the MASP during the winter (characterized as dry season), however, its occurrence

66  in the north and northwest of São Paulo state also has been reduced due to control measures (Valente and Laurini, 2021). In

67  addition to the significant levels of pollutants generated locally or regionally, increasing events of transport of biomass burning

68  from the Amazon and Central parts of Brazil have been observed in the MASP at the end of the decade (Pereira et al., 2021;

69  Miranda et al., 2017), occurring mainly in the drier periods (July-October) (Vieira et al., 2023). Local biomass burning was

70  pointed out as relevant, including the burning of charcoal and wood in barbecue and pizzerias and waste burning (Kumar et

71  al., 2016). In 2014 and 2015, biomass-burning sources were apportioned and found to explain nearly one-fourth of particulate

72  matter in the dry season (Pereira et al., 2017b; Emygdio et al., 2018).

73  The São Paulo State Environmental Company (CETESB) monitors legislated pollutants at 26 air quality stations

74  throughout the MASP. Despite the efforts of local governments to improve air quality in the region, in 2019, they all recorded

75  concentrations of PM$_{2.5}$ above the value recommended by the WHO, reaching critical levels in the drier months (April to

September). Considering the aspects mentioned before, it is crucial to periodically update the chemical characterization of particulate matter since Brazilian environmental agencies do not carry out such extensive monitoring. It can be said that particle sources in São Paulo always need to be studied and identified, but this depends on good quality chemical composition data. The composition of aerosols varies with the changing fleet and the policies concerning the burning of biomass. Furthermore, they are also influenced by the changing climate and meteorological conditions. In recent years, dryer weather conditions in the winter have favored forest and crop fires in central Brazil and the accumulation of pollutants (Souto-Oliveira et al., 2023; Pereira et al., 2021). This study aimed to thoroughly characterize $PM_{2.5}$ chemical composition and toxicity in the MASP, identifying the relative contribution of emission sources. Associations with weather conditions and case studies of air pollution events were also investigated. The adoption of receptor models was performed to study the emission sources of $PM_{2.5}$, and these results were associated with particle size distributions.

## 2 Materials and methods

### 2.1 Sampling of $PM_{2.5}$ and particle number size distributions monitoring

High-volume samplers (Energética, Brazil) (1.13 $m^3$ $min^{-1}$ flow) were employed to collect $PM_{2.5}$ on the rooftop of the Institute of Chemistry building at the University of São Paulo, in the city of São Paulo, Brazil (23°33'53"S, 46°43'32"W), located in a green area, and more than 2 km away from a busy expressway (Marginal Pinheiros) (Figure 1). The sampling occurred between June 04 and September 12, 2019, in a pre-lockdown polluted period, starting six months before the pandemic. During this campaign, a dark precipitation event (August 19) was observed, an unprecedented event that was termed "black rain" following biomass burning episodes in central South America (Pereira et al., 2021). Ninety-nine samples were collected for 24 hours (starting at 9 AM, local time). Quartz fiber filters (20 cm × 25 cm, Whatman, UK) were employed to collect $PM_{2.5}$. These filters were decontaminated before sampling by heating at 600 ℃ for 6 h. Before and after sampling, the filters were weighed in a microbalance (controlled temperature and humidity for equilibrium: T = 25 ℃ and RH = 50%). Then, the filters were wrapped into a laminated sheet and stored at 5 ℃ to avoid volatilization and reactions of the analytes before the analysis (de Oliveira Alves et al., 2015; Souza et al., 2014).
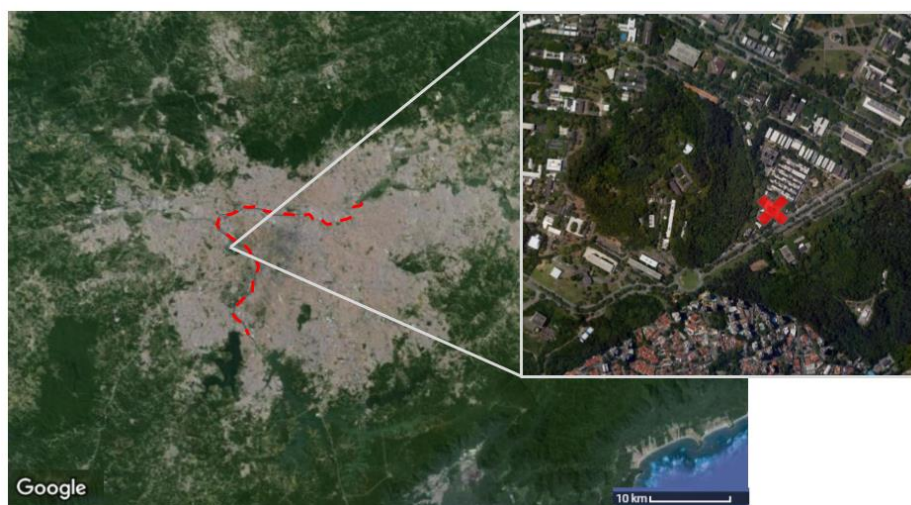
**Figure 1:** Sampling site location (marked with red cross) (© Google Maps). Heavily trafficked expressways are indicated with the red dashed line.

Particle number size distributions (PNSD) were monitored using a Scanning Mobility Particle Sizer (SMPS 3081, TSI Inc) in association with a Condensation Particle Counter (CPC 3010, TSI Inc). The system provided particle number size

105 distributions in the size range from 10 to 450 nm every 2 min. PNSD measurements were averaged to match the filter sampling

106 periods. Average distributions were also calculated for periods of interest in the dataset. The SMPS data were collected on the

107 rooftop of the Institute of Astronomy, Geophysics, and Atmospheric Sciences of the University of São Paulo, 500 meters from

108 the Institute of Chemistry. PNSD measurements were taken between June and September 2019, totalizing 48 non-consecutive

109 sampling days during the austral winter.

110 **2.2 Analytical procedures**

111 Distinct chemical composition analyses were performed. Thus, pieces of the filters were sent to each laboratory. At the Institute

112 of Chemistry (University of São Paulo), water-soluble ions (WSI) and PAHs were determined. The extraction of WSI from

113 filters (4 cm$^2$) was performed with 10 mL of deionized water (Milli-Q, Merck Millipore, USA) under sonication for 15 min.

114 Then, extracts were filtered with syringe filters (Millex-GV, 0.22 µm, PVDF), and cations and anions were quantified in an

115 ion chromatograph (Modules 819, 830, 833, 818, and 820, Metrohm, Switzerland). Anions F$^-$, Cl$^-$, NO$_2^-$, Br$^-$, NO$_3^-$, PO$_4^{3-}$,

116 SO$_4^{2-}$, C$_2$O$_4^{2-}$, HCO$_2^-$, and C$_4$H$_2$O$_4^{2-}$, and cations Ca$^{2+}$, Mg$^{2+}$, K$^+$, NH$_4^+$, and Na$^+$ were quantified. Pereira et al. (2023a) describe

117 the adopted columns and eluents. Fluka (Switzerland) analyte standards were used. Recoveries fell between 80-120% and were

118 obtained by adding known concentrations of standards to blank filters, which are reported in Table S1.

119 Punches of approximately 20 cm² from the filters underwent extraction using ultrasonic baths with 80 mL of

120 dichloromethane for three cycles of twenty minutes, as described by Pereira et al. (2017a). The extracts were concentrated via

121 rotary evaporation under low pressure (at 35°C for approximately 30 minutes) and fractionated on a chromatographic column

122 packed with 1.5 g silica gel. The methodology described in Vasconcellos et al. (2010) was modified and adopted in this study,

123 involving three elutions: the first fraction carried alkanes (10 mL of hexane), while the second (9.6 mL of hexane + 5.4 mL of

124 toluene), and the third (7.5 mL of hexane and 7.5 mL of dichloromethane) carried PAHs and their derivatives. The second and

125 third fractions were combined to enhance recovery. The fractionated extracts were concentrated by rotary evaporation under

126 reduced pressure (at 35°C for approximately 15 minutes), filtered, stored in 2 mL vials, dried, and reconstituted with 0.5 µL

127 of hexane. Samples were diluted prior to analysis by gas chromatography coupled with mass spectrometry (GC/MS, Agilent,

128 GC 7820A, and MS 5975), using an Agilent VF-5ms column (stationary phase, 30 m × 0.250 mm × 0.25 µm), with helium as

129 the carrier gas (99.97% purity and flow rate of 1.0 mL min$^{-1}$). The following species were determined: phenanthrene (Phe),

130 anthracene (Ant), fluoranthene (Flt), pyrene (Pyr), retene (Ret), benzo(a)anthracene (BaA), chrysene (Chr),

131 benzo(b)fluoranthene (BbF), benzo(k)fluoranthene (BkF), benzo(e)pyrene (BeP), benzo(a)pyrene (BaP), indene(1,2,3-

132 c,d)pyrene (InP), dibenzo(a,h)anthracene (DBA) and benzo(g,h,i)pyrene (BPe) and coronene (Cor). Recovery was assessed by

133 adding known quantities of PAHs mix to filters containing 15 mg of the certified material (Urban Dust SRM 1649b, NIST,

134 USA). Most species presented values between 80 and 120%, averaging 100% (Table S1).

135 Carbonaceous species (OC and EC) in the quartz fiber filters were determined through thermal-optical analysis using a

136 *Sunset Laboratory Inc.* carbon analyzer at the Institute of Physics of the University of São Paulo. The EUSAAR-2 temperature

137 protocol (Cavalli et al., 2010) was employed, and the transmittance-based pyrolysis correction was applied, similar to previous

138 studies conducted in the MASP (Monteiro dos Santos et al., 2016). Temperature-resolved carbon fractions are obtained, with

139 increasing temperatures: four for organic fractions (OC1 to OC4, from higher to lower volatility temperatures), four for

140 elemental carbon (EC1 to EC4), and the organic pyrolyzed carbon (PC) is monitored. Total OC is the sum of OC1, OC2, OC3,

141 OC4, and PC, while total EC is the sum of EC1, EC2, EC3, and EC4, subtracted by PC. The first stage in helium medium is

142 carried out under the following conditions of temperature and time steps: 200 °C for 120s (OC1), 300 °C for 150s (OC2),

143 450 °C for 180s (OC3) and 650 °C for 180s (OC4). In the second stage, under He-O$_2$ medium, the four steps are: 500 °C for

144 120s (EC1), 550 °C for 120s (EC2), 700 °C for 70s (EC3) and 850 °C for 80s (EC4). Secondary organic carbon (SOC) was

145 estimated considering the 5$^{th}$ percentile of the OC/EC ratios, similar to Monteiro dos Santos et al. (2016). Organic matter (OM)

146 was calculated as $1.6 \times$ OC, adopted for urban aerosols (Turpin and Lim, 2001).

147 Quartz fiber filters were subjected to acid digestion using a microwave digester oven (CEM MDS-2000, USA) at the

148 Institute of Geosciences of the University of São Paulo. A strip of 20 cm × 2.5 cm of the filter was submitted to digestion in a

149 closed vessel (PFA) with a mixture of $HNO_3$ and $H_2O$ (10 and 15 mL, respectively), then the volume was adjusted to 50 mL.

150 Major and trace elements were quantified by inductively coupled plasma mass spectroscopy (ICP-MS, model iCAP Q, Thermo

151 Fisher Scientific, USA). The percent recoveries and detection limits were previously reported for all the determined analytes

152 and reported in Pereira et al. (2023a).

153 At the Center for Environmental and Marine Studies (CESAM) of the University of Aveiro (Portugal), sugar species

154 were extracted from the filters with ultrapure Milli-Q water in ultrasonic agitation, as described by Oduber et al. (2021). After

155 the extraction, the solutions were filtered with syringe filters (PTFE; 0.2 μm) and transferred to vials for liquid chromatography

156 analysis with amperometric detection. Sugar compounds such as levoglucosan (Lev), mannosan (Man), galactosan (Gal),

157 mannitol (Mnt), arabitol (Ara), and xylitol (Xyl) were determined with a Thermo Scientific Dionex™ ICS-5000 equipped with

158 an anion-exchange analytical column (CarboPac® PA-1; 2 × 250 mm). Multi-step gradient conditions were adopted, with

159 ultrapure Milli-Q water and two solutions of NaOH (200 mM and 5 mM). Recoveries were reported by Caseiro et al (2007).

## 2.3 Benzo(a)pyrene equivalent indexes

161 Benzo(a)pyrene equivalent indexes were calculated to evaluate toxicity parameters due to exposure to PAHs. Equations 1 and

162 2 were employed to calculate the $BaP_{TEQ}$ and $BaP_{MEQ}$ by multiplying each species' concentrations by their toxic and mutagenic

163 equivalency factors (TEF and MEF), as reported in de Oliveira Alves et al. (2020). The PAH carcinogenicity equivalent index

164 ($BaP_{Eq}$) was also calculated by applying Equation 3, incorporating specific PAH concentrations as adopted by Yassaa et al.

165 (2001) and Cecinato (1997).

166 $$BaP_{TEQ} = ([BaA] \times 0.1)+([Chr] \times 0.01)+([BbF] \times 0.1)+([BkF] \times 0.1)+([BaP] \times 1)+([InP] \times 0.1)+([DBA] \times 5)+ ([BPe] \times 0.01) \tag{1}$$

167 $$BaP_{MEQ} =([BaA] \times 0.082)+([Chr] \times 0.017)+([BbF] \times 0.25)+([BkF] \times 0.11)+([BaP] \times 1)+([InP] \times 0.31)+([DBA] \times 0.29)+ ([BPe] \times 0.19) \tag{2}$$

168 $$BaP_{Eq}=([BaA] \times 0.06)+([BbF] \times 0.07)+([BkF] \times 0.07)+([BaP] \times 1)+([DBA] \times 0.6)+([InP] \times 0.08) \tag{3}$$

## 2.4 Data treatment and Positive Matrix Factorization

170 Pearson coefficients were obtained to estimate the correlation between different variables (Jamovi software), and $r$ was

171 considered significant when $p < 0.05$. Correlations between 0.0 and 0.3 were considered negligible, between 0.3 and 0.5 as

172 weak, between 0.5 and 0.7 as moderate, between 0.7 and 0.9 as strong, and between 0.9 and 1.0, as very strong (Khan et al.,

173 2018). To evaluate equal and unequal variances, the Mann–Whitney U test was also employed ($p < 0.05$). Polar plots were

174 constructed with mass concentrations as wind speed and direction functions. They are obtained by a function in the OpenAir

175 package (RStudio). Diagnostic ratios were performed between two (or more) chemical species concentrations: OC/EC, EC/Cu,

176 PC/CTot, Fe/$Ca^{2+}$, Cu/Sb, Cu/Zn, Fe/Cu, Sn/Sb, La/Ce, V/Ni, Pb/Cu, Cu/$Ca^{2+}$, BaP/(BaP+BeP), Flt/(Flt+Pir), InP/(InP+BPe),

177 BaA/(BaA+Cri), LMW-PAHs/HMW-PAHs, Pyr/BaP, Pyr/BbF, Flt/BbF, $NO_3^-$/EC, $SO_4^{2-}$/$NO_3^-$, $SO_4^{2-}$/EC, $K^+$/Lev, Lev/Man,

178 $SO_4^{2-}$/Zn, and $NO_3^-$/Zn.

179 The ISORROPIA model calculates the composition and phase state of the water-soluble inorganic aerosol in

180 thermodynamic equilibrium with gas phase precursors, simulating the process of dissolution of atmospheric particles and the

181 ion formation (Bian et al., 2014; Fountoukis and Nenes, 2007; Li et al., 2014; Vieira-Filho et al., 2016a). In this study, the

182 ISORROPIA II was applied. It can solve two types of problems: (i) forward (or "closed system") and (ii) reverse (or "open

183 system"). The reverse problem approach was adopted in this study using aerosol phase concentrations of $NH_3$ (as ammonium

184 ion), $H_2SO_4$, $Na^+$, $Ca^{2+}$, $K^+$, $Mg^{2+}$, HCl, and $HNO_3$ to estimate water content, salt aerosol concentrations, and gaseous precursors

185 aerosols. The aerosol-atmosphere system was considered thermodynamically stable (with precipitation of salts).

The enrichment factor (EF) is an approximation employed to identify the degree to which an element in the aerosol is enriched or depleted (da Rocha et al., 2012). EF was calculated using aluminum as a soil tracer, according to crustal element abundances described in the Appendix of Lee (1999). Elements with EF below 10 are of crustal origin (not enriched), and elements with EF above 10 are of non-crustal origin (anomalously enriched) (Pereira et al., 2007). Equation 4 is adopted to calculate EF, where $C_{Xp}$ and $C_{Alp}$ are the concentrations of elements X and Al in the sample, and $C_{Xc}$ and $C_{Alc}$ are their average concentrations in the Earth's crustal material:

$$EF = \frac{\frac{C_{Xp}}{C_{Alp}}}{\frac{C_{Xc}}{C_{Alc}}} \qquad (4)$$

The positive matrix factorization (PMF) receptor model, including ninety-four samples, was applied to the datasets (Paatero and Tapper, 1994). The USEPA PMF5.0 software was used. The variable classification followed the established definitions: "bad" when the signal-to-noise ratio (S/N) was below 0.2, "weak" with S/N between 0.2 and 2, and "strong" when S/N was above 2 (Lang et al., 2015). The number of samples below the detection limit (Amato et al., 2016; Contini et al., 2016; Paatero and Hopke, 2003) and the thermal stability of the species (Pereira et al., 2017b) were also considered. Weak variables had their uncertainty increased by three times, and bad variables were excluded from the model (Norris et al., 2014). Twenty-two species were considered as strong ($NH_4^+$, $K^+$, $NO_3^-$, $SO_4^{2-}$, V, Mn, Ni, Zn, As, Rb, Cd, Sb, Pb, Lev, OC1, OC2, OC3, OC4, PC, EC1, EC2, and EC3), six species were classified as weak ($Ca^{2+}$, $Mg^{2+}$, Cu, EC4, LMW-PAHs, and HMW-PAHs) and the concentrations of particulate matter were defined as a total variable (weak). Concentrations below the detection limits (DL) were substituted by half of the DL value. Uncertainties were calculated following the procedure by Norris et al. (2014). To evaluate the number of factors, Q robust ($Q_R$) was compared to Q theoretical value ($Q_T$) as in Pereira et al. (2017b). The final model was obtained with an additional 7% modeling uncertainty. Solutions with three to eight factors were tested, and a final solution with five factors was taken as the best result, with factors that could be well interpreted. Bootstrap mapping (BS) and displacement of factor analysis (DISP) were used to analyze factor solutions, confirming a 5-factor solution as the most feasible. Most markers used to identify the sources were within the BS interquartile ranges (box), and mapping ranged from 87%-100%. Furthermore, no DISP swaps were observed.

## 2.5 Backward air mass trajectories

For specific pollution events, backward air mass trajectories spanning 48 hours were generated using the HYSPLIT model (Draxler and Rolph, 2003) via the READY (Real-time Environmental Applications and Display System) platform provided by NOAA (National Oceanic and Atmospheric Administration). Trajectory frequencies were calculated to illustrate the origin of air masses reaching the MASP in selected polluted periods, starting at 9:00 AM (local time). The trajectories were calculated at the heights of 500 and 3000 meters above ground level (AGL), based on GDAS meteorological fields with 1-degree resolution.

## 2.6 Ecotoxicity assays

The ecotoxicity of PM$_{2.5}$ was screened by the kinetic version of the *Aliivibrio fischeri* bioluminescence-based assay (Kováts et al., 2021). This bioassay mimics the respiratory metabolism of biological systems resulting from exposure to particulate matter. This assay provides an easy-to-quantify endpoint to assess the presence of toxic substances. Inhibition of the bacteria's metabolism by toxic substances is demonstrated by the attenuation of its natural light emittance. Two 17 mm diameter filter sections were cut and ground in an agate mortar. The samples were then transferred to 4 mL vials, to which 2 mL of ultra-pure water was added. The suspensions were prepared with continuous agitation. The manufacturer's reconstitution solution was used to rehydrate the lyophilized bacteria (strain NRRL-B-11177, from Lange Co.), which were then stabilized for 35 min at

224 12°C. For each sample, serial dilutions in 2% NaCl were prepared in 96-well plates. After adding the bacterial suspensions to

225 the samples, the bioluminescence intensity was continuously read for the first 30 seconds by a Luminoskan Ascent

226 Luminometer (Thermo Scientific). The bioluminescence was reread after 30 min of contact. The Ascent Software (Aboatox

227 Co., Finland) was employed to calculate the EC50 (concentration that causes 50% inhibition of bioluminescence compared to

228 the control). Depending on their toxic units (TU = 100/EC50%), samples were cataloged as non-toxic (TU < 1), toxic (1 < TU

229 < 10), very toxic (10 < TU < 100), or extremely toxic (TU > 100).

## 230 3 Results and discussions

### 231 3.1 PM$_{2.5}$ chemical composition and general trend

232 The concentrations of particulate matter presented a wide variation. PM$_{2.5}$ concentrations ranged from 7 to 47 µg m$^{-3}$, averaging

233 24 µg m$^{-3}$ (Figure 2a) and exceeding the new World Health Organization's (WHO) daily recommendations on 75% of sampling

234 days (15 µg m$^{-3}$). However, no national or local limits were surpassed (CONAMA, 2018; WHO, 2021). The period was

235 characterized by low precipitation, and the variation of meteorological conditions (temperature, relative humidity, pressure,

236 and irradiance are described in the SI (Figure S1). In terms of mass fractions, the most abundant elements observed in the 2019

237 intensive campaign were K > Al > Cu > Fe (Table 1). These species are linked to dust resuspension, vehicular sources, and

238 biomass burning. Potassium (K) is attributed to soil resuspension and biomass burning, aluminum (Al) is related to soil

239 resuspension, and iron (Fe) and copper (Cu) are associated with vehicular sources in the MASP (Brito et al., 2013; Pereira et

240 al., 2017b, 2023a, 2023b). Biomass burning tracer levoglucosan (Lev) increased in specific periods (Figure 2b) and will be

241 further discussed. As observed in the 2014 intensive campaign, secondarily formed ions were the most abundant: $NO_3^- > SO_4^{2-}$

242 $> NH_4^+$ (Figure 2c and 2d). However, the profile has changed slightly, showing a greater abundance of nitrate over sulfate in

243 most of the period, unlike the intensive campaigns of 2008, 2010, 2013, and 2014 (Table S2), when sulfate was predominant

244 in PM (Pereira et al., 2019, 2017a,b, Souza et al., 2014). The total mass of the most common element oxides was estimated

245 ($Al_2O_3$, $SiO_2$, $TiO_2$, MnO, and $Fe_2O_3$). Since Si was not determined in this study, $SiO_2$ was estimated based on the Al content

246 (as three times the concentrations of $Al_2O_3$) (Alves et al., 2018). The sum of these oxides can be used to estimate the proportion

247 of crustal species in the PM$_{2.5}$ (Almeida et al., 2006) and accounted for 7%.

248

249
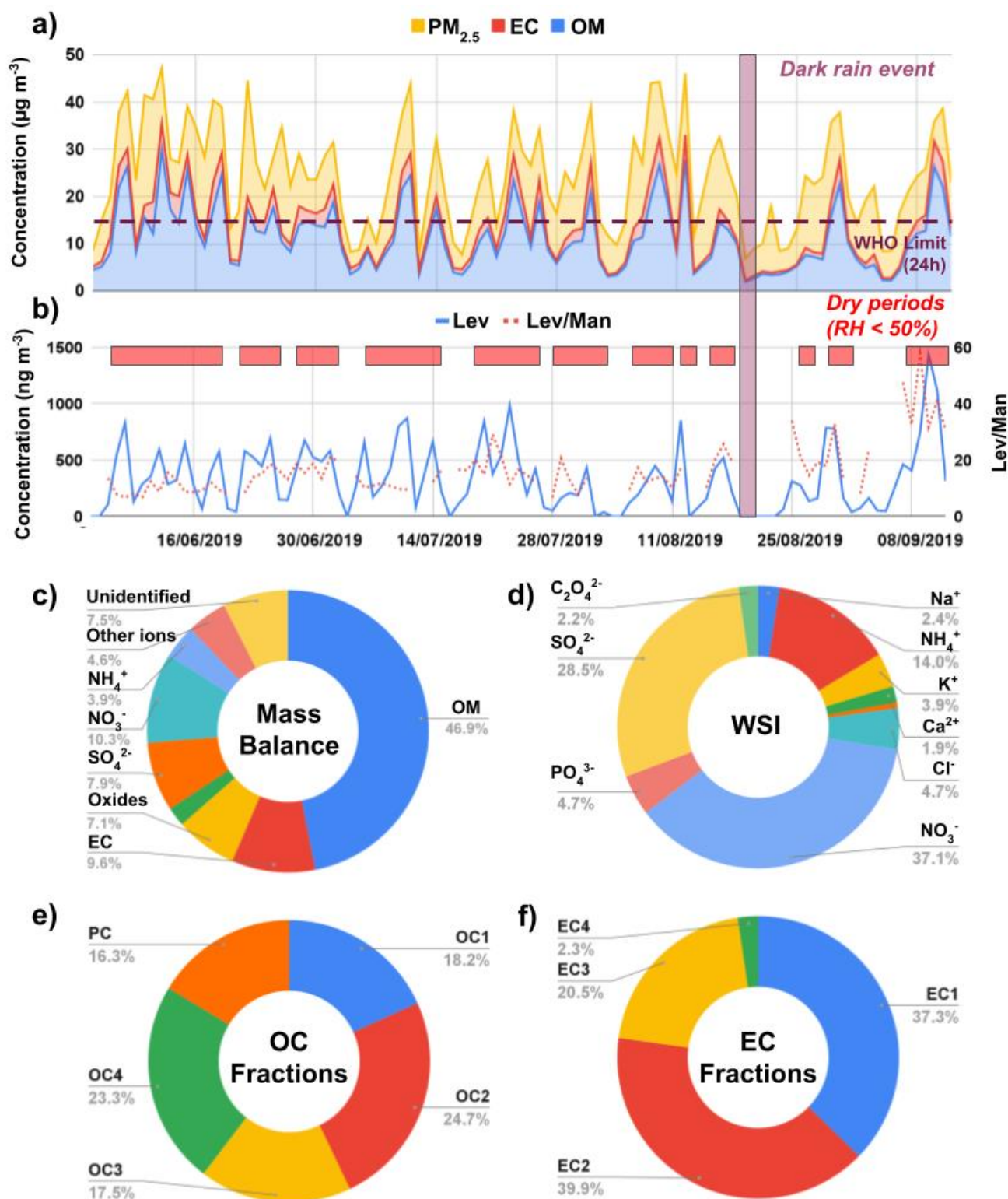
**Figure 2:** Daily variation in the concentrations of **(a)** PM$_{2.5}$ (the upper line gives concentrations and yellow area corresponds to non-carbonaceous PM$_{2.5}$), OM, and EC (stacked blue and red areas, respectively), and **(b)** Lev and Lev/Man ratio, **(c)** fractions of OC and **(d)** EC, **(e)** ionic composition, and **(f)** mass balance. In **(b),** "Dry periods" are marked with red squares (daily minimum RH < 50%), and the dark rain event is marked with the purple box.

254

255 **Table 1:** Median, average, minimum, and maximum concentrations of different species and diagnostic ratios[1].

| | Med. | Ave. | Min. | Max. | (Cont.) | Med. | Ave. | Min. | Max. |
|---|---|---|---|---|---|---|---|---|---|
| **($\mu$g m$^{-3}$)** | | | | | | | | | |
| **PM$_{2.5}$** | 23.7 | 24.5 | 6.9 | 47.2 | **Cu** | 93 | 136 | 13 | 931 |
| **OC** | 6.3 | 7.2 | 1.2 | 18.6 | **Zn** | 39 | 49 | 4.0 | 250 |
| **EC** | 1.8 | 2.3 | 0.3 | 6.7 | **As** | 1.2 | 1.2 | 0.3 | 2.9 |
| **SOC** | 2.7 | 3.4 | 0 | 10.6 | **Se** | 1.1 | 1.4 | 0.1 | 5.7 |
| **(ng m$^{-3}$)** | | | | | **Rb** | 1.8 | 2.2 | 0.1 | 6.2 |
| **Na$^+$** | 143 | 166 | 5 | 549 | **Sr** | 4.6 | 5.2 | 0.3 | 15.4 |
| **NH$_4^+$** | 737 | 954 | 61 | 4241 | **Mo** | 1.6 | 4.9 | 0.1 | 31.2 |
| **K$^+$** | 247 | 268 | 6 | 686 | **Ag** | 0.27 | 0.26 | 0.01 | 0.85 |
| **Ca$^{2+}$** | 101 | 128 | 17 | 517 | **Cd** | 0.49 | 0.66 | 0.03 | 2.69 |
| **Mg$^{2+}$** | 44 | 43 | 6 | 95 | **Sn** | 5.5 | 8.2 | 0.2 | 30.7 |
| **Cl$^-$** | 174 | 321 | 14 | 1505 | **Sb** | 3.8 | 5.7 | 0.3 | 27.9 |
| **NO$_3^-$** | 2115 | 2531 | 134 | 10711 | **Ba** | 14 | 16 | 4 | 54 |
| **PO$_4^{3-}$** | 320 | 318 | 36 | 784 | **La** | 0.25 | 0.29 | 0.01 | 1.47 |
| **SO$_4^{2-}$** | 1651 | 1942 | 69 | 6139 | **Ce** | 0.23 | 0.26 | 0.01 | 2.09 |
| **C$_2$O$_4^{2-}$** | 158 | 152 | 12 | 319 | **Tl** | 0.06 | 0.07 | 0.00 | 0.23 |
| **(ng m$^{-3}$)** | | | | | **Pb** | 11 | 14 | 1 | 38 |
| **Lev** | 315 | 380 | 38 | 1437 | **Bi** | 0.16 | 0.2 | 0.01 | 0.9 |
| **Man** | 23 | 29 | 7 | 123 | **U** | 0.23 | 0.25 | 0.06 | 0.69 |
| **Gal** | 13 | 16 | 7 | 41 | **Ratios** | | | | |
| **Xyl** | 6 | 8 | 2 | 75 | **OC/EC** | - | 3.1 | 1.1 | 10.2 |
| **(ng m$^{-3}$)** | | | | | **EC/Cu** | - | 17.3 | 2.2 | 146.5 |
| **Al** | 180 | 208 | 11 | 1142 | **Fe/Ca$^{2+}$** | - | 0.8 | 0.0 | 7.8 |
| **K** | 271 | 286 | 16 | 757 | **Cu/Sb** | - | 23.6 | 3.6 | 543.1 |
| **Ti** | 7.5 | 8.9 | 1.4 | 141 | **Cu/Zn** | - | 2.8 | 0.2 | 23.1 |
| **V** | 1.2 | 1.7 | 0.1 | 8.0 | **Fe/Cu** | - | 0.7 | 0.0 | 6.8 |
| **Cr** | 1.7 | 3.4 | 0.0 | 20.7 | **La/Ce** | - | 1.1 | 0.5 | 16.7 |
| **Mn** | 6 | 6.9 | 0.6 | 25 | **V/Ni** | - | 0.8 | 0.1 | 2.8 |
| **Fe** | 64 | 99 | 2 | 674 | **SO$_4^{2-}$/NO$_3^-$** | - | 0.8 | 0.0 | 4.9 |
| **Co** | 0.07 | 0.08 | 0.00 | 0.33 | **K$^+$/Lev** | - | 0.7 | 0.0 | 4.7 |
| **Ni** | 1.5 | 2.0 | 0.2 | 27 | **Lev/Man** | - | 13 | 6.7 | 58 |

256

257     A predominance of organic matter was observed in PM$_{2.5}$, accounting for a mass fraction of 47%, on average, followed
258 by NO$_3^-$ and EC (each accounting for 10%) (Figure 2c). OM and EC represented a significant fraction of PM$_{2.5}$, over 50% on
259 average. Similarly, in the Eastern part of São Paulo (2019-2020), organic matter (OM) corresponded to nearly 40% of PM$_{2.5}$
260 (Vieira et al., 2023). Previous studies (2008 and 2014) pointed to higher proportions of EC in PM$_{2.5}$ (Table S2). The elemental
261 carbon fraction is reducing worldwide (Chow et al., 2022a, Yamagami et al., 2019) (more details are presented in the SI), and

---

[1] Average diagnostic ratios were calculated with the average species' concentrations.

a reduction trend of vehicular emissions of this species was observed in the MASP (Pereira et al., 2023a, 2023b). The emission limits following a control program policy were upgraded in the early 2010s, similar to Euro 5 and Euro 4, for heavy-duty (HDVs) and light-duty vehicles (LDVs), respectively (Pacheco et al., 2017) and more recently in 2022 (CETESB, 2022). The control policies are associated with reducing carbonaceous species, especially EC (Pereira et al., 2023a,b). Furthermore, adopting biofuels (e.g., ethanol and biodiesel blends) reduces these pollutants' emissions (de Abrantes et al., 2009). The relative reduction of sulfate and EC levels is observed worldwide, as reported in the SI. Following a similar trend to the observed in other Latin American metropolises (Gómez-Peláez et al., 2020), the precursor $SO_2$ reduced relatively more than $NO_x$ in the MASP in the last decades (Andrade et al., 2017), and its concentrations were eight-fold lower in 2019 compared to 2000 (Figure S2) (CETESB, 2020). The transport sector became the dominant $SO_2$ source in the MASP from the 1980s to the early 2000s after the reduction of industrial emissions following the adoption of electrical boilers (Kumar et al., 2016). Since the early 2010s, S10 diesel and S50 gasoline have been adopted to control vehicular emissions, although older trucks were allowed to use S500 diesel (CETESB, 2015). From 2024, a resolution will establish new national specifications for road-use diesel oils, discontinuing S500 fuels totally (MME, 2024). Due to these reductions in the MASP, sulfate vehicular emissions were estimated to be fivefold lower than those from stationary sources in 2019 (CETESB, 2020).

The OC and EC fractions are shown in Figures 2e and 2f, respectively. A predominance of OC2 and OC4 was observed among the organic carbon fractions and EC1 and EC2 among the elemental carbon fractions. The relatively low proportion of EC3 suggests that this site is less affected by HDV emissions since previous experiments in the MASP have shown that EC3 predominated in a diesel-powered HDV-impacted tunnel (Pereira et al., 2023b; Monteiro dos Santos et al., 2016). In the tunnel studies, the OC2 fraction dominated the emissions and had already been observed in urban areas of São Paulo in 2013 (Monteiro dos Santos et al., 2016). OC1 is the most volatile fraction, which may explain its relatively lower proportion in the particulate matter. Pyrolyzed carbon (PC) represented 16% of OC. Previously, PC represented 20-30% of total OC at the university and downtown sites, accounting for less than 10% of OC in a street canyon (Monteiro dos Santos et al., 2016). This fraction encompasses oxygenated components and links to water-soluble organic carbon (WSOC), secondary formation, and primary sources, including biomass burning (Zhu et al., 2014; Pio et al., 2007; Yu et al., 2002). More recently, it has been connected to HDV emissions, possibly due to the adoption of biodiesel (Pereira et al., 2023b).

Levoglucosan, a monosaccharide anhydride widely used as a biomass-burning tracer, presented the highest average concentration (380 ng m$^{-3}$) among isomer sugars, followed by mannosan (29 ng m$^{-3}$). Compared to a previous intensive campaign (2014), the average K$^+$ level reduced from 809 ng m$^{-3}$ to 268 ng m$^{-3}$ (almost three-fold), while levoglucosan presented a similar level (509 ng m$^{-3}$) (Pereira et al., 2017). Since potassium levels are high in crop-burning emissions (Chow et al., 2022a), the significant reduction in concentrations may be due to the lower influence of sugarcane burning. Control policies have contributed to the decrease in the number of fires (Valente and Laurini, 2021). Galactosan was present in less than half of the samples, averaging 16 ng m$^{-3}$. It is usually observed in lower proportions than mannosan in biomass burning emissions (Bhattarai et al., 2019). It is possible to observe in the trajectory cluster a predominance of air masses coming from the north and northwest and a low influence of trajectories passing through the ocean (nearly 20%) (Figures 3a and 3b). This indicates the importance of the transport of biomass burning aerosols from rural areas of São Paulo state and central region of Brazil (nearly 50%) during this period. The highest levoglucosan concentrations were observed on September 10 and 11 (1437 and 1119 ng m$^{-3}$) in a dry period that preceded a cold front. Relatively higher concentrations were also observed for K$^+$ on both days (543 and 555 ng m$^{-3}$). Back trajectory frequencies arriving at 500 m for these two days point to the typical influence of air masses from the north and northwest of São Paulo state (Figures 3c and 3d), as observed in previous campaigns (Pereira et al., 2017a, 2017b). When a height above the boundary layer is considered (3000 m), it is possible to see a frequency of trajectories passing through areas in the country's central region. The states of Minas Gerais and Goiás, located north of São Paulo state, also presented many fires from September 10 to 12 (Figure S3) (INPE, 2019).
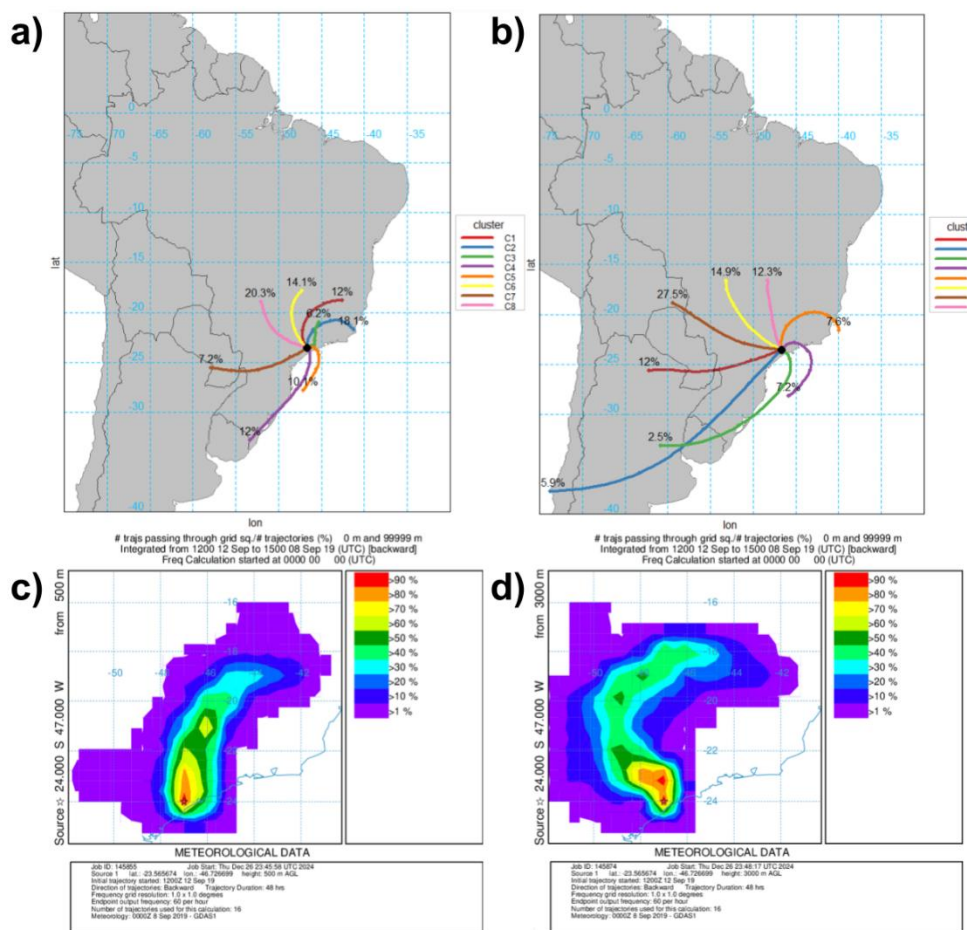
**Figure 3:** Backward trajectory clusters for the sampling period, arriving at **(a)** 500 m and **(b)** 3000 m, and trajectory frequencies for September 10 and 11, 2019, arriving at **(c)** 500 m and **(d)** 3000 m.

Xylitol was the most detected polyol, with an average concentration of 8 ng m$^{-3}$. This species is mainly found in biological material, soil biota, and biomass-burning smoke (Marynowski and Simoneit, 2022; Gonçalves et al., 2021; Caseiro et al., 2007). Gonçalves et al. (2021) found a relation between this polyol and biomass-fuelled heating, reporting an increase from 2.95 ng m$^{-3}$ in summer to 19.9 ng m$^{-3}$ in winter in an urban background site in Portugal. However, much lower concentrations were observed in an urban site near sugarcane plantation areas in the north and northwest of São Paulo state (below 2 ng m$^{-3}$) (Carvalho et al., 2023). Back trajectories were obtained for a period with high xylitol levels, which peaked at 75 ng m$^{-3}$ on August 30 (Figure S4). These trajectories indicate an influence of air masses from the north and northwest of São Paulo state, corroborating a biomass burning contribution to this species (Figure S5). Relatively high xylitol was also observed on September 10 and 11 (above 25 ng m$^{-3}$), when the highest levoglucosan concentrations were observed. Other polyols were detected in a few samples, as discussed in SI. Arabitol and mannitol levels tend to increase in the wet season, unlike biomass-burning tracers, as observed in a medium-sized city in the São Paulo state (Carvalho et al., 2023). The studied period is expected to present lower pollen-related emissions since these emissions are enhanced under higher temperatures and humidity (Marynowski and Simoneit, 2022).

The total concentration of PAHs in PM$_{2.5}$ ranged from 1.1 to 37.3 ng m$^{-3}$, with an average of 10.1 ng m$^{-3}$, higher than the observed in the 2019 extensive campaign (including a wet period), of 4.7 ng m$^{-3}$ (Serafeim et al., 2023). The most abundant compounds observed in the present study were BbF, BeP, and BPe (Figure 4 and Table S3). BbF is potentially carcinogenic and related to emissions from gasoline-powered vehicles (Ravindra et al., 2008), and its predominance is often observed in São Paulo (Pereira et al., 2017a,b). This compound is emitted in smaller amounts by LDVs than BaP (Pereira et al., 2023a).

325 However, it is less influenced by chemical decomposition and is more persistent (Aubin and Farant, 2000). Along DBA, this
326 species presents the longest residence times in the atmosphere among PAHs (Keyte et al., 2013).
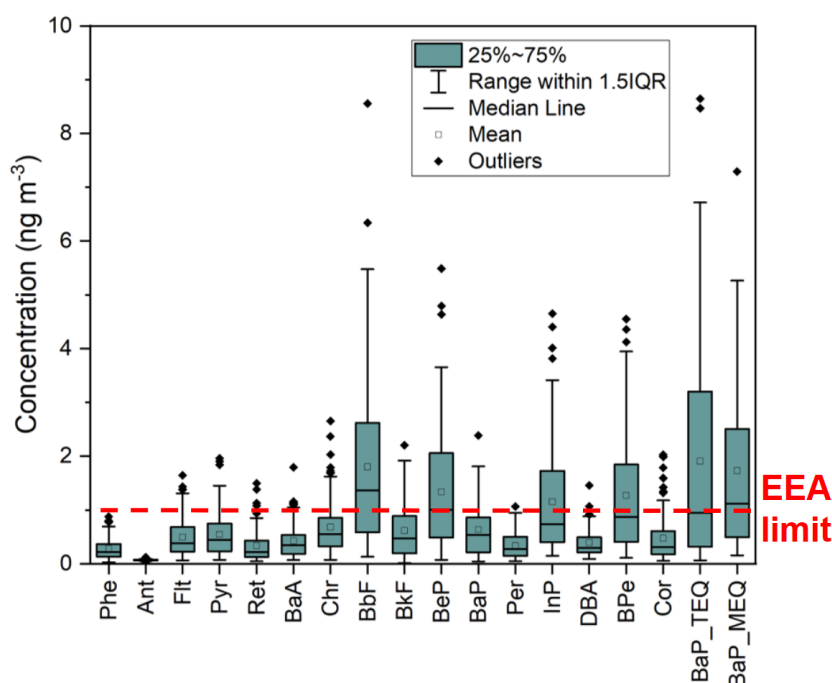
327

328 **Figure 4:** Box plots of polycyclic aromatic hydrocarbon concentrations. The dashed red line indicates EEA's
329 recommended annual limit for BaP.

330      Benzo(a)pyrene averaged 0.6 ng m$^{-3}$ (ranging from 0.04 to 2.39 ng m$^{-3}$) and surpassed the annual limit recommended
331 by the European Environment Agency (EEA; 1 ng m$^{-3}$) in 16% of the samples (Ravindra et al., 2008). However, half of the
332 samples exceeded this value if the BaP toxicity equivalent index (BaP$_{TEQ}$) is considered (average of 1.9 ng m$^{-3}$ and range of
333 0.06-8.64 ng m$^{-3}$). The benzo(a)pyrene-equivalent index (BaP$_{Eq}$), calculated according to Yassaa et al. (2001), ranged between
334 0.04 and 4.08 ng m$^{-3}$ (average of 0.9 ng m$^{-3}$). BaP$_{Eq}$ was lower than those determined for samples collected in previous winter
335 campaigns in São Paulo (ranging from 1.1 to 3.4 ng m$^{-3}$ in 2010, 2012, 2013 and 2014) (Pereira et al., 2017b, 2017a). This
336 reduction may be attributed to emission regulations and adopting biofuels, such as ethanol and biodiesel, which can lower
337 HMW-PAH emissions (de Abrantes et al., 2009; Pereira et al., 2023a). This trend follows a reduction in PAH emissions in
338 recent decades in developed countries due to the establishment of new regulations (Shen et al., 2011). BaP$_{MEQ}$ and BaP$_{TEQ}$
339 tended to increase with northern and northwestern winds, more associated with drier weather, stable conditions, and biomass-
340 burning-related aerosols (Figure S6). The opposite was observed with S and SE winds when cold fronts and sea breezes were
341 registered.

## 3.2      Diagnostic ratios and polar plots

343 The OC/EC ratios in the present study ranged from 1.1 to 10.2, with an average of 3.1 (the monthly averages varied from 3.0
344 to 3.3) (Figure S7a). In previous studies in the MASP, ratios lower than 1 were often observed in tunnels and roadside
345 experiments. These ratios increased to nearly 2 in greener, low-traffic sites, characterized by increased biogenic influence and
346 secondary formation (Brito et al., 2013; Monteiro dos Santos et al., 2016; Pereira et al., 2023b). The distance to main roads
347 can increase the ratios and values between 1.8 and 3.7 are found in background sites (Amato et al., 2016). However, biomass
348 burning can also increase this ratio, reaching over 4.1-14.5 (Watson et al., 2001; Wu et al., 2018). Notably, the monthly average
349 values obtained in the present study were higher than those found in intensive campaigns in the same sampling site in 2014,

350 2013, 2010, and 2008 (1.2-2.3)[2]. These previous campaigns were conducted in similar dry periods, but in shorter monitoring

351 periods (Pereira et al., 2019; Pereira et al., 2017a,b; Souza et al., 2014). The ratio increase between these years may indicate a

352 more significant influence of biofuel consumption and reduction of EC emissions (Dawidowski et al., 2024; Pereira et al.,

353 2023a) since the ethanol sales in the state of SP in 2019 were 75% higher than in 2013 (MME, 2023). Furthermore, an enhanced

354 contribution from secondary organic carbon (SOC) formation may also contribute to this. SOC was estimated to reach nearly

355 half of OC, with a maximum of 83% (Table 1). The formation of SOC is enhanced under higher concentrations of oxidants

356 such as ozone, which was observed in the MASP after 2006 (Andrade et al., 2017). In Santiago, Chile, there is a trend of

357 increasing photochemical activity and oxidizing capacity in the atmosphere (2001-2018), leading to an increase in the

358 secondary fraction of aerosols (Menares et al., 2020). The enhancement of SOC under a more oxidative atmosphere and/or

359 higher temperatures requires further investigation.

360       Polar plots were obtained to investigate associations between wind direction and diagnostic ratios (Figure 5). The

361 OC/EC ratios appeared to increase with relatively stronger SE winds (Figure 5a). These winds can also transport biogenic

362 organic carbon from forested areas near the coast and air pollutants from coastal petrochemical and harbor areas. In the

363 southeastern parts of MASP, more influenced by forests, less volatile oxidized organic aerosols were predominant and

364 associated with SOC derived from VOCs emitted by biogenic and vehicular sources (Monteiro dos Santos et al., 2021).

365 Furthermore, humidity can favor the partition of more polar SOC, as enhanced RH can lead to water uptake by hygroscopic

366 submicron particles (Satsangi et al., 2021).

367

368

---
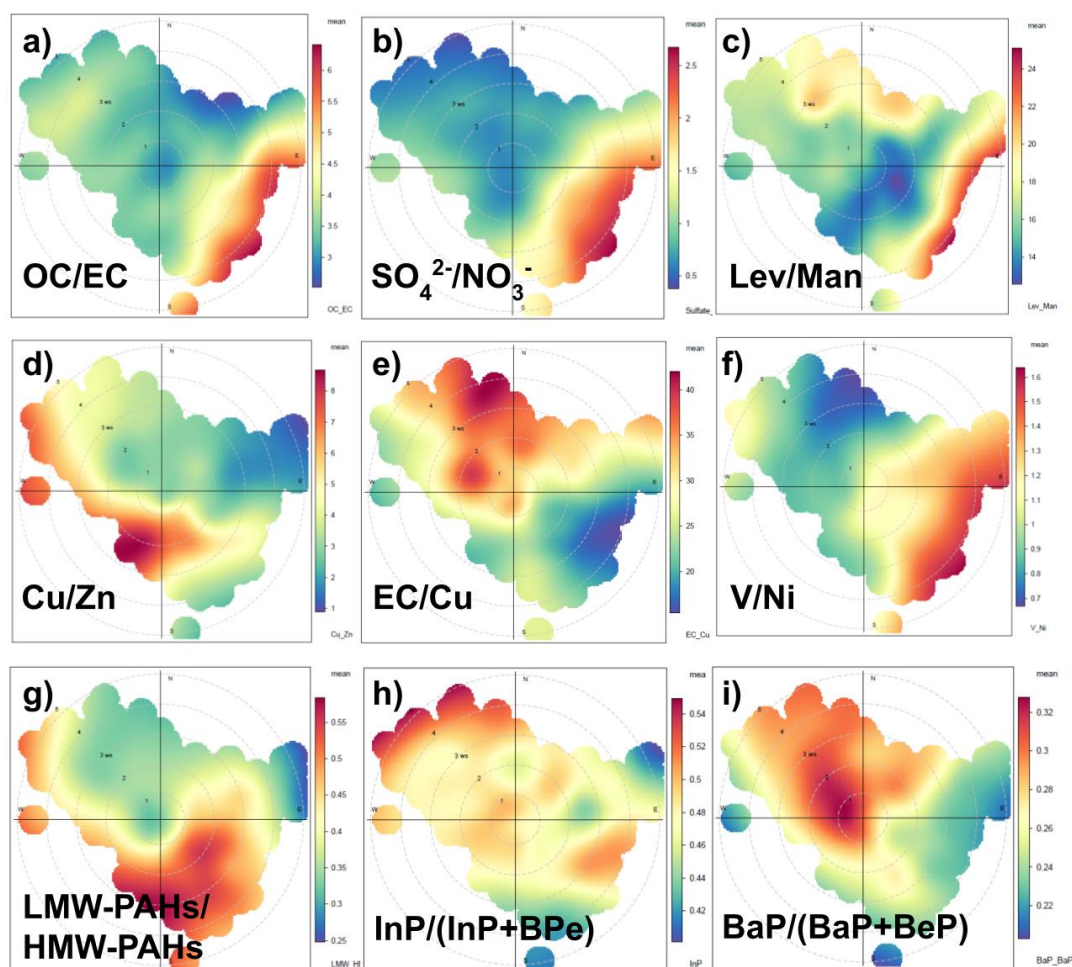
[2] Ratios (OC/EC and Lev/Man) were obtained for $PM_{10}$ in 2010 and 2013, assuming that most of these species are found in the fine fraction in São Paulo.

**Figure 5:** Polar plots considering the diagnostic ratios as a function of wind speed and direction for the ratios OC/EC **(a)**, $SO_4^{2-}/NO_3^-$ **(b)**, Lev/Man **(c)**, Cu/Zn **(d)**, EC/Cu **(e)**, V/Ni **(e)**, LMW-PAHs/HMW-PAHs **g)**, InP/(InP+BPe) **(h),** and BaP/(BaP+BeP) **(i).** Distance from the center is related to wind speed, and ratios increase from blue to red.

The average $SO_4^{2-}/NO_3^-$ in this study was 0.8 (0.04-4.6), lower than the 1.6 (from July to December) of the 2019 extensive study (Serafeim et al., 2023). The difference can be attributed to the lower temperatures in the present study (from June to September), less favorable to the volatilization of particulate nitrate (Tang et al., 2016). In 2014, higher ratios were observed, reaching 1.2 in the intensive period and 2.2 in the extensive period (Pereira et al., 2017b). The ratio in the 2008 intensive campaign was higher than in 2014 (1.8) (Souza et al., 2014). Besides the ambient temperature, the reduction in this ratio can be associated with the more accentuated reduction of sulfur dioxide levels if compared to nitrogen oxides (Sect. 3.1). The ratio $SO_4^{2-}/NO_3^-$ appeared to increase with SE and E winds (Figure 5b). This suggests that the sulfate production may be favored by humid and cloudier conditions associated with these air masses. Additionally, this can be attributed to an influence of sulfur dioxide sources in the southeastern and eastern parts of the MASP (e.g., industries and HDVs). Sulfate particles can be formed by the growth of the condensation mode with the addition of sulfate and water in the aerosol droplet process (Guo et al., 2010). The southeastern part of MASP is influenced by industrial sources, and high sulfate levels are linked with locally emitted $SO_2$ (Monteiro dos Santos et al., 2021).

Galactosan and mannosan are products of hemicellulose thermal decomposition, while levoglucosan is formed during the combustion of cellulose (Simoneit, 2002). Since the amount of cellulose and hemicellulose varies with biomass type (hardwood contains relatively higher amounts of cellulose), the Lev/Man ratio can distinguish the smoke from different biofuels (Li et al., 2021; Zhu et al., 2015). Typical ranges of 15–25 and 3–10 have been documented for hardwood and softwood burning, respectively (Li et al., 2021). The average Lev/Man in the present study was 13 (6.7 - 58.0), slightly higher than averages observed in 2014, 2013, and 2010 (ranging from 8 to 12)[1] (Pereira et al., 2017a,b, 2019). Previous ratios were closer to the values found in chamber sugarcane burnings (Lev/Man = 10) and areas impacted by this type of smoke plumes (Lev/Man = 9) (Hall et al., 2012; Urban et al., 2014). In an agroindustrial region in northern São Paulo state, a change in the Lev/Man ratio was observed in 2020 (Lev/Man = 19) (Scaramboni, 2023). This increase was attributed to a change in the biomass burning profile. Over the past decade, there has been a reduction in the burning of sugarcane straw and an increased use of sugarcane bagasse in power plants in the last decade (MME, 2024). This shift, alongside the increased contribution of forest fires and other agricultural residue burnings, can play a significant role in this trend. During high levoglucosan events in September, under lower relative humidity (Figure 2), the Lev/Man ratios surpassed 40, suggesting the influence of different types of biomasses. In areas impacted by forest fires in the Amazon, likely linked to hardwood burning, the ratios ranged from 15 to 24 (Decesari et al., 2005; Graham, 2002). Furthermore, in central Brazil, burning grass in the *cerrado* (tropical savanna biome) resulted in relatively lower amounts of mannosan since this biomass contains less mannose than hardwood (Scaramboni et al., 2024). Before the dark precipitation event registered on August 19, associated with smoke transported from areas in central Brazil and the Amazon (Pereira et al., 2021), Lev/Man values also exceeded 20.

The median $K^+$/Lev ratio was 0.7, considerably lower than that observed in the 2014 dry period (1.6) (Pereira et al., 2017a). Lower $K^+$/Lev ratios, typically below 1, have been found in emissions from wood stove combustion and forest fires (Caseiro et al., 2009). Jung et al. (2014) reported similar $K^+$/Lev ratios for hardwood and softwood burning (0.04 and 0.02, respectively)[2], but this ratio was higher for crop burning (averaging 1.9)[2]. Urban et al. (2012) documented an average ratio of around 4 for fine sugarcane-burning particles[3], justifying this value with the enrichment of $K^+$ in the leaves and the inefficient formation of levoglucosan during the flaming phase. The reduction in the proportion of $K^+$/Lev in the present study may be associated with reducing sugarcane burning after regulation. Some $K^+$/Lev peaks were observed on days with very low Lev concentrations (06/17, 07/27, 07/28, 08/06, and 09/01) (Figure S7b), suggesting the influence of soil-related $K^+$.

---

[3] These authors presented the ratios as Lev/$K^+$.

The Lev/Man ratio increased with stronger winds, whether from S/SE or N (Figure 5c), denoting the influence of emissions from burning various types of biomasses. If the polar plot is obtained with Conditional Probability Function (CPF) and Non-parametric Wind Regression (NWR), the increase under stronger N winds is prominent (Figure S8a and S8b). The lowest ratios were found with low-speed SE winds, probably due to wood burning in some restaurants in that area. Brazilian pizzerias traditionally use eucalypt logs in wood stoves. However, recently, briquettes have been adopted (Lima, 2015). Sun et al. (2019) reported Lev/Man ratios in the range of 17-19 for different types of briquettes. Some authors found Lev/Man ratios mostly below 10 for woodstove emissions from different types of wood logs, while briquettes presented ratios of 29.7 in hot start and 1.4 in cold start conditions (Gonçalves et al., 2011).

The diagnostic ratios EC/Cu, Fe/Cu, Cu/Zn, and Cu/Sb were associated with the proportion of LDVs and HDVs in tunnels in the MASP (Pereira et al., 2023b). In previous studies, EC was more related to HDV emissions, while Cu was linked to LDV emissions (Brito et al., 2013). EC/Cu ratios in the present varied between 2 and 146, and the average ratio was 17. These values approached those observed for LDVs (5-8) rather than the ratios associated with a more HDV-impacted fleet (80-189). Sb has been described as a tracer of abrasion sources, including brake wear (Thorpe and Harrison, 2008). Cu is also present in Brazilian exhaust emissions from ethanol/gasohol vehicles (Brito et al., 2013). The present average Cu/Sb ratio was 24 (4-543), higher than the median values observed in tunnels (11-14). This difference may be attributed to the distance of the sampling site from a high-traffic area and a lower contribution from brake abrasion sources. The average Cu/Zn was 2.8 (0.2-23.1), falling between the median value observed for LDV (6.2) and that documented for HDV+LDV-impacted tunnels (0.9). The Cu/Zn and Cu/Sb ratios increased with southern weak winds (Figures 5d and S8c), suggesting an enrichment in copper and predominance of LDV emissions in this area, possibly associated with the traffic of vehicles in the nearby residential neighborhood. On the other hand, the EC/Cu and Fe/Cu ratios increased with N winds (Figures 5e and S8d), which may indicate an influence of HDVs passing in the expressway located north of the campus.

The average V/Ni ratio was 0.8 (0.1-2.8). Higher values for residual fuel oil combustion are found, ranging from 1 to 3 (Johnson et al., 2014). This ratio increased with strong E/NE/SE winds (Figure 5f), suggesting an influence from oil burning in industries located in these areas (Vieira et al., 2023; Souto-Oliveira et al., 2021). The La/Ce ratio, similarly to the latter, was favored by S/SE winds (Figure S9h). Higher ratios (4.3) were observed for fluidized-bed catalytic cracking (FCC) during petroleum refining, while a lower value (0.7) was documented for automobile catalyst emissions (Kulkarni et al., 2006). A petrochemical complex in the southeastern area of the MASP may explain this influence (Caumo et al., 2022; Gioia et al., 2017). Previous studies have identified isotopic fingerprints from the Cubatão petrochemical complex, an industrial area outside the MASP, following the passage of cold fronts and the arrival of southeastern winds (Souto-Oliveira et al., 2018).

Diagnostic ratios between PAHs for the analyzed samples were calculated and shown in Table S3. BaP/(BaP+BeP) values lower than 0.5 indicate that the analyzed particles were aged, as BaP undergoes photolysis more quickly than BeP (Tobiszewski and Namieśnik, 2012). The median was equal to 0.32, suggesting a predominance of aged particles. In three samples (collected on 27/07, 03/08, and 28/08), this ratio was close to 0.5, indicating fresh emissions. The Flt/(Flt+Pir) median was 0.48. According to De La Torre-Roche et al. (2009), values of this ratio ranging from 0.4 to 0.5 are characteristic of the burning of fossil fuels. InP/(InP+BPe) median ratio was equal to 0.48, similar to what was observed in 2014 by Pereira et al. (2017b). Values between 0.2 and 0.5 are associated with emissions from the burning of fossil fuels (Yunker et al., 2002). The BaA/(BaA+Cri) presented an average of 0.38, falling near the observed for vehicular sources (0.2-0.35) (Akyüz and Cabuk, 2010).

ΣLMW-PAHs/ΣHMW-PAHs median ratio was 0.35, within the range reported for pyrogenic (<1) emissions by some authors (Zhang et al., 2008). However, this ratio was previously found to vary with the proportions of LDVs and HDVs (0.7 and 7.5, respectively) (Pereira et al., 2023b) and temperature (Tobiszewski and Namieśnik, 2012). The ratios Pyr/BaP, Pyr/BbF, and Flt/BbF were associated with the proportion of LDVs and HDVs, increasing with the latter (Pereira et al., 2023b).

Nevertheless, the ratios can be influenced by the volatilization of Pyr and Flt in warmer conditions and the photodegradation of BaP. The values were similar to those observed for gasoline emissions (near or below 1).

ΣLMW-PAHs/ΣHMW-PAHs and Pyr/BaP ratios appeared to be affected by winds coming from NW (Figures 5g and S8e), with mixed biomass burning and vehicular influence. These ratios also increase under cooler winds from the S, which may favor the condensation of LMW-PAHs in the particulate phase (Ravindra et al., 2008). Temperature is observed as the meteorological parameter that most affects total and individual PAHs, with a more substantial influence on LMW-PAHs (Amarillo and Carreras, 2016). InP/(InP+BPe) ratios approached the values (above 0.5) found for grass, wood, and coal combustion with NW winds (Figure 5h) (Yunker et al., 2002). It was not possible to observe the same for Flt/(Flt+Pyr) (Figure S8f), which increased with S and SE winds. This suggests a relation between the cooler/cloudier conditions and the shorter photochemical residence time of Pyr compared to Flt (Keyte et al., 2013). The highest BaP/(BaP+BeP) values were registered for lower wind speeds (Figure 5i), suggesting fresh local emissions (Tobiszewski and Namieśnik, 2012), although this ratio also seemed to increase with stronger NW winds.

**3.3    Source apportionment (PMF)**

The factor profiles obtained by Positive Matrix Factorization are shown in Figure 6. A five-factor solution was obtained, attributed to biomass burning (BB), secondary formation (SF), and industries (IN), and two were associated with vehicular emissions (VE1 and VE2). Factor 1 (BB) was characterized by biomass-burning-related species such as levoglucosan, $K^+$, and some carbonaceous species (Bhattarai et al., 2019; Simoneit, 2002). However, the presence of Cd, Sb, and Pb suggests a mixture with vehicular sources (Thorpe and Harrison, 2008) or that these species may be linked with waste burning (La Colla et al., 2021). This factor was also characterized by a significant contribution from pyrolyzed carbon (PC), which is linked to water-soluble organic carbon (WSOC) often associated with biomass burning and secondary organic aerosol (Yu et al., 2002; Zhu et al., 2014). Recently, it has been observed that the biomass burning factor can mix with secondary organic carbon contribution in a Korean industrial area (Han et al., 2023). Among elemental carbon fractions, EC1 was the most abundant. Some elements, such as Rb, also appeared in the biomass burning profile. This species has been described as a component of some types of soil by Calvo et al. (2013), wood-burning emissions (Fine et al., 2001), and biomass burning aerosols in the Amazon (Artaxo et al., 1994). Recently, water-soluble rubidium in fine particulate matter has been assigned to wood-burning emissions and considered an alternative biomass burning tracer (Massimi et al., 2020). This factor increased with winds coming from N and NW, indicating the influence of the transport of biomass burning aerosols from agro-industrial areas in São Paulo state and potentially from forested areas in northern and central Brazil. It decreases with S and SW winds, suggesting a reduction with cold fronts and sea breezes (Sánchez-Ccoyllo et al., 2002). The results agree with the study of Souto-Oliveira et al., (2023), which showed the impact of the transport of wildfires to the MASP during fine particulate matter exceedance events in 2020.
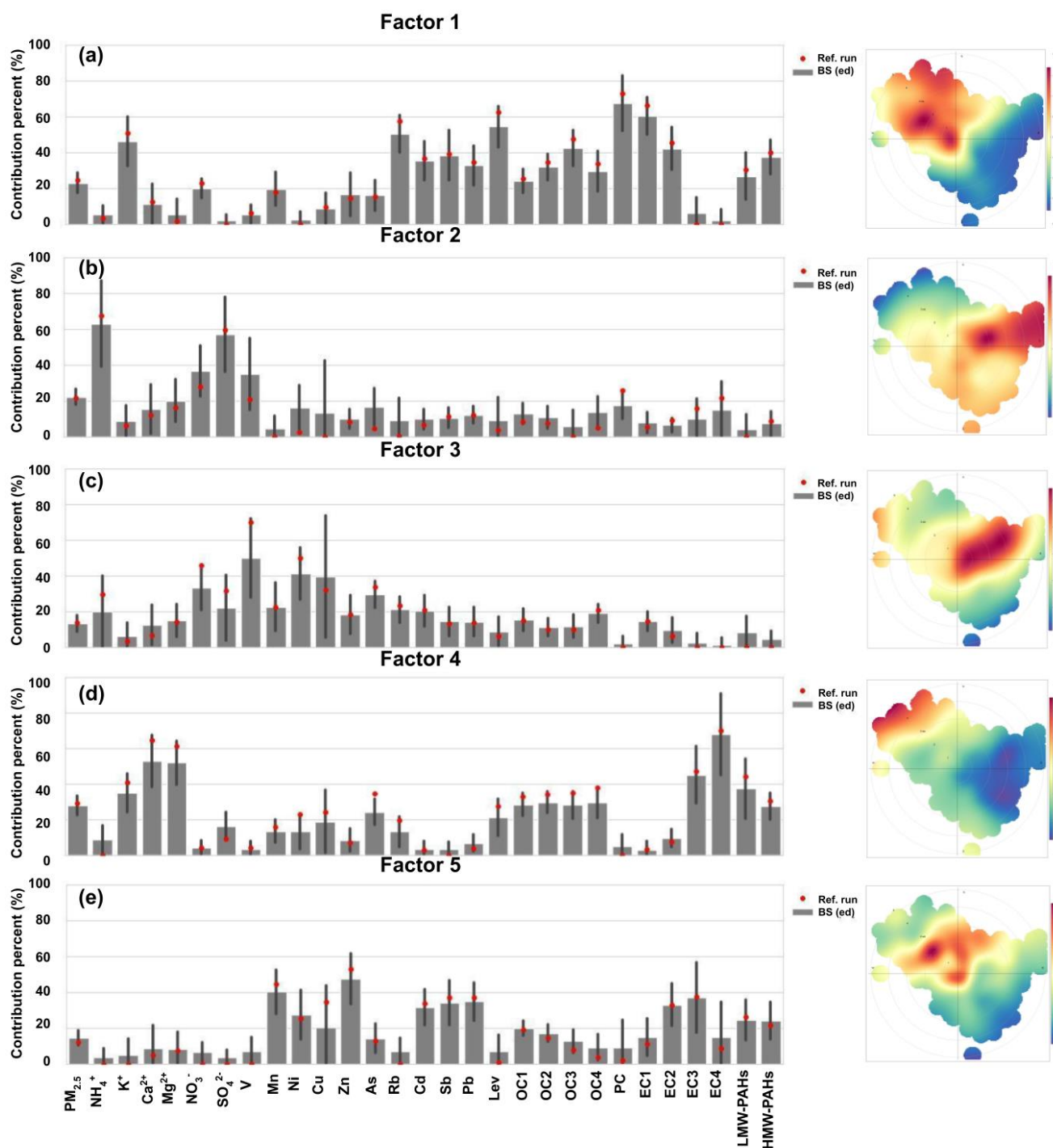
**Figure 6:** Profiles identified with the PMF receptor model and polar plots **(a-e)**. Model reference runs (Ref. run) are marked in red, bootstrap runs (BS), and standard deviation (sd) in grey.

Factor 2 (SF) was highly loaded with secondary formation species, mainly $NH_4^+$ and $SO_4^{2-}$. This process likely involves the oxidation of sulfur dioxide, the formation of sulfuric acid, neutralization with ammonia, and the production of ammonium sulfate (($NH_4$)$_2SO_4$) (Han et al., 2023; Iannielo et al., 2011). Furthermore, this factor also presented loadings of some primary emission species, such as vanadium. Serafeim et al. (2023) also observed high loadings for Ni and V in the secondary-related factor in the MASP. These species originate from industrial emissions (Calvo et al., 2013). Previously, it has been observed with the WRF-Chem model that secondary formation explains 20 to 30% of $PM_{2.5}$ in the MASP (Vara-Vela et al., 2016), increasing in the summertime (Pereira et al., 2017b). The SF factor was previously attributed to vehicular-related emissions in a previous study in 2014 (Pereira et al., 2017). However, with the reduction of $SO_2$ emissions by vehicular sources (CETESB,

2020), the industries' contribution has become relevant (Section 3.1). However, most industries are located on the outskirts, whereas vehicular emissions are more concentrated in the city's central areas. Thus, the apportionment of secondary sulfate formation can be a subject for further studies.

Factor 3 (IN) showed high V, Ni, and nitrate loads. Earlier studies in the MASP have associated Ni and V with residual oil burning and industrial sources (Andrade et al., 1994; Castanho and Artaxo, 2001). Heavy oil combustion in industrial boilers also emits nickel and zinc, especially in the ultrafine fraction (smaller than 0.1 μm) (Jang et al., 2007; Linak et al., 2004). Factor 3 (IN) increased with the same wind direction as Factor 2 (SF), which suggests that it may be partially related to secondary formation. This is possibly due to emissions of precursor gases, such as $NO_x$ and $SO_2$, or associated with the same air masses. Secondary aerosol formation can mislead the separation of factors in PMF, as observed by Faisal et al. (2024).

Factor 4 (VE1) was loaded with soil resuspension constituents, such as $Ca^{2+}$ and $Mg^{2+}$, as well as with species previously related to vehicular emissions in the MASP, such as As and Cu, carbonaceous species (OC1, OC2, OC3, OC4, EC3, and EC4), LMW-PAHs, and HMW-PAHs (Pereira et al., 2017b, 2023a, 2023b). In the extensive 2019 campaign, a single road dust factor represented 32% of $PM_{2.5}$ (Serafeim et al., 2023). The association with construction-related calcium, found in concrete, can also be considered (Bourotte et al., 2006). EC3 and EC4 were abundant in this factor. EC3 was anteriorly related to HDV emissions in MASP, while EC4 was found in an urban canyon. Furthermore, OC2, OC3, and OC4 were found in LDV emissions in similar proportions (Monteiro dos Santos et al., 2016; Pereira et al., 2023a). Levoglucosan was also observed in a smaller proportion in this factor. As observed in 2014, this factor overlaps with the BB factor (Pereira et al., 2017b), as they increase with the same wind direction. However, the contribution of VE1 increases with NW stronger winds, corroborating effect of road dust resuspension. Strong NW winds are often attributed to prefrontal conditions (Ribeiro et al., 2018). Another aspect contributing to the overlap is that this anhydrosugar is also found in the $PM_{10}$ from the wear between tires and pavements, given that wheel rubbers have cellulose in their composition (Alves et al., 2020). However, $PM_{2.5}$-bound levoglucosan is emitted in much smaller proportions by this non-exhaust vehicle emission source compared to biomass burning (Bhattarai et al., 2019). This "hybrid" factor may occur because the aerosols in the urban atmosphere, comprised mainly of vehicular-related species, road dust, and biomass burning smoke, arrive mixed at this semi-background site. Additionally, it is challenging to differentiate HDV from LDV emissions in this site (Pereira et al., 2017a). The increase in time resolution for PMF can reduce mixing in source profiles, decreasing sample variability (Wang et al., 2018). This improvement can be achieved through real-time techniques (e.g., Aerosol Chemical Speciation Monitor) (Monteiro dos Santos et al., 2021). The contribution of non-exhaust emissions, such as road dust resuspension, is expected to increase in the future (Thorpe and Harrison, 2008) as exhaust emissions are on a downward trend due to increasingly stricter regulations and improved treatment systems.

Factor 5 (VE2) presented several species of vehicular origin, such as Mn, Ni, Cu, Zn, Sb, and the potentially toxic species Cd and Pb (Brito et al., 2013; Pereira et al., 2023a). OC and EC fractions were also found in this factor, particularly EC3, associated with HDVs (Pereira et al., 2023b). This vehicular factor increased with lower wind speed, suggesting a local contribution. The site is located next to an avenue with a constant flow of buses and LDVs during the daytime and is near a busy expressway. Despite the lower proportion, the emissions of buses and trucks contributed to almost half of the black carbon levels observed in the MASP (Brito et al., 2018). In the Scanning Electron Microscopy (SEM) study performed by Bourotte et al. (2006), particles rich in carbon, copper, and zinc were identified and associated with incomplete fossil fuel burning. Zinc is also enriched in tire wear particles, as zinc oxide is added to the tires in the vulcanization process (Thorpe and Harrison, 2008). Copper was previously assigned to LDV exhaust emissions and to the corrosion of the internal parts of the MASP fleet engines (Ferreira da Silva et al., 2010). This species was also pointed out as a brake dust particle tracer (Thorpe and Harrison, 2008).

Figure 7 shows the contributions of each type of source to $PM_{2.5}$ and their variation between sampling days. Biomass burning accounted for 25% of $PM_{2.5}$. This contribution was slightly higher than that documented in the intensive campaign of

2014 (18.3%). In the extensive study performed in 2019 (including dry and wet seasons), the biomass burning factor represented 13% of ambient PM$_{2.5}$, a similar share to that observed in the 2014 extensive period (Pereira et al., 2017b; Serafeim et al., 2023). However, it is lower than the observed in the present study since the period from June to September is typically more affected by biomass burning (Pereira et al., 2017a). In a major city in central Brazil (Cuiabá), biomass burning was relevant and represented one-third of PM$_{10}$ (Parra et al., 2024). Several peaks of the BB factor coincided with lower RH values. An increase in the contribution of this factor was observed two days before the sky-darkening phenomenon at MASP on August 19, when the occurrence of dark precipitation was attributed to pollutants emitted by biomass burning (Pereira et al., 2021). Overall, crop burning and wildfires can explain a significant share of PM$_{2.5}$ in this period. However, the regional biomass burning profile is changing, with reduced sugarcane straw burning, increased contribution of wildfires, and sugarcane bagasse use as fuel, as discussed in Section 3.2. The study of Knorr et al. (2017) predicts that due to climate change, levels of wildfire-related PM$_{2.5}$ can rise to dangerous levels during fire seasons in many regions, including parts of South America. This increase in PM$_{2.5}$ levels can occur even with accentuated reductions of other anthropogenic emissions. In the last decade, wildfire smoke has influenced PM$_{2.5}$ trends across much of the US, including major cities, complicating efforts to control this pollutant (Buchholz et al., 2022). In temperate regions, the high contribution of biomass burning to PM$_{2.5}$ in the winter can be attributed to residential heating (Nava et al., 2020). In the temperate metropolis of Beijing (China), biomass and coal burning can represent nearly half of PM$_{2.5}$ in winter, as these sources are used for heating and cooking in nearby rural areas (Srivastava et al., 2021). Due to regulations, open-field burning in China has become less frequent. However, biomass burning for home heating in northern China can affect downwind areas such as South Korea (Cheong et al., 2024).
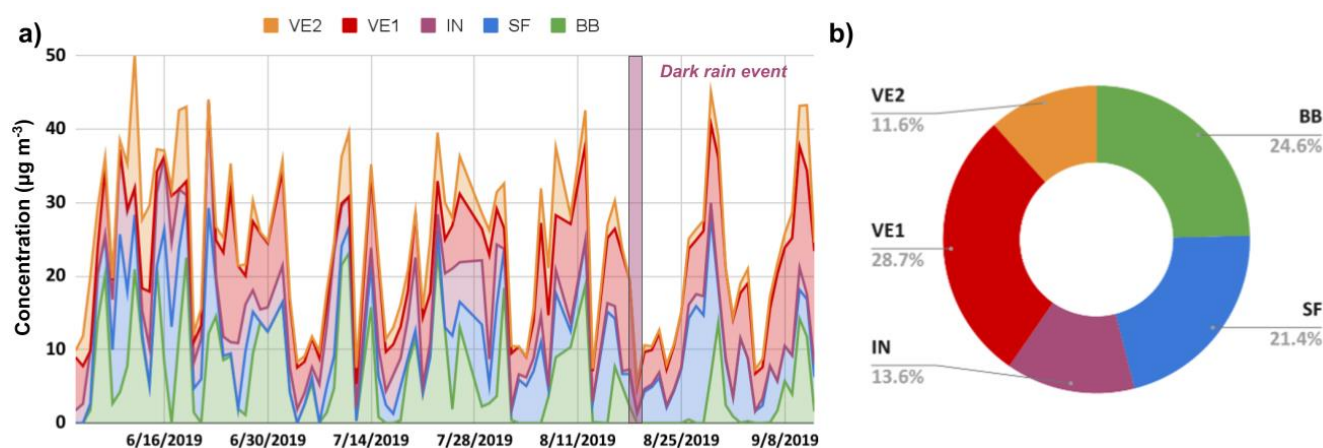
**Figure 7:** Daily factor contribution **(a)** and PM$_{2.5}$ contributions **(b)** identified with the PMF receptor model.

The vehicular-related sources, VE1 (29%) and VE2 (12%), represent a significant share of particulate matter in the city (over 40%). Vehicular sources were dominant in 2013, 2014, and 2015 (Souto-Oliveira et al., 2021; Emygdio et al., 2018; Pereira et al., 2017a). Previous studies were performed in other Brazilian cities, where vehicular emissions ranged from 3% to nearly half of PM$_{2.5}$ (Rio de Janeiro, Vitória, and Recife). Sea spray was found as relevant in Brazilian coastal sites (Galvão et al., 2019; Justo et al., 2023; dos Santos et al., 2014). Despite the entrance of sea breezes on a few occasions, it was not possible to identify this source in the present study. As discussed in Section 3.1, a few trajectories passed by the ocean. The factor VE1 increased throughout the sampling period and dominated PM$_{2.5}$ at the end of August and the beginning of September, indicating greater dust resuspension at the end of winter due to the long dry spell and higher wind speeds (Figure S9). In another source apportionment study performed in the east region of São Paulo in 2019, four factors were found to contribute to PM$_{2.5}$: heavy-duty vehicles (42%), light-duty vehicles (9.9%), soil and local particles (38.7%) and local sources (8.6%) (Vieira et al., 2023), with a higher share of vehicular sources than the present study and an increase of soil particles in the dry season. According to

572  Serafeim et al. (2023), vehicular emissions and biomass burning were associated with enhanced oxidative potential. Secondary
573  formation (SF) of aerosol from oxide precursors, which can be emitted from vehicular and industrial sources, represented 21%
574  of PM$_{2.5}$ Industrial sources accounted for only 13.6%, a similar level to that observed in 2014 (over 10%) (Pereira et al., 2017b).
575  A relatively low impact of industrial emissions is felt in this part of the city. Most industries are now located on the MASP's
576  outskirts and in other metropolitan areas in the state (Kumar et al., 2016), and there are no large industries near the sampling
577  site. Industrial sources can be relevant in other Brazilian cities. Pelletizing and steel industry contributed to more than 60% of
578  PM$_{2.5}$ in Vitória (Galvão et al., 2019). The Simplified Quantitative Transport Bias Analysis (SQTBA) approach was utilized,
579  recognizing the plume dispersion process and considering it as part of back trajectory analysis. The contribution of the IN
580  factor, combined with the frequencies of the trajectories, suggested an influence from areas located to the east and northeast
581  (Figure 8a), including parts of the MASP and other neighboring metropolitan areas with a high concentration of industries
582  (Figure 8b).
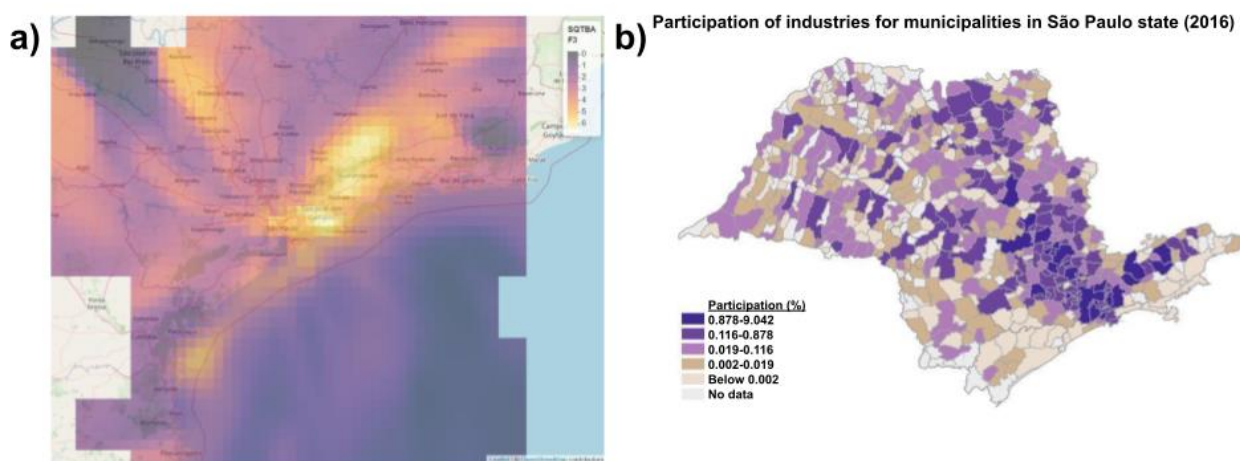
584  **Figure 8: (a)** Trajectory analysis for the contribution of factor 3, and **(b)** participation of industries for municipalities
585  in São Paulo state (industrial transformation value), adapted from SEADE (2019).

587  **3.4     Correlations between PMF results and other variables**

588  The factors obtained with the PMF receptor model were correlated with other variables: meteorological data (temperature,
589  relative humidity, and wind) collected from the local station, concentrations of chemical species, diagnostic ratios, and results
590  obtained from the ISORROPIA thermodynamic model (modeled solid and liquid inorganic aerosol, water content, NaNO$_{3(s)}$,
591  Na$_2$SO$_{4(s)}$, NaHSO$_{4(s)}$, NaCl$_{(s)}$, NH$_4$Cl$_{(s)}$, NH$_4$NO$_{3(s)}$, (NH$_4$)$_2$SO$_{4(s)}$, NH$_4$HSO$_{4(s)}$, CaSO$_{4(s)}$, Ca(NO$_3$)$_{2(s)}$, CaCl$_{2(s)}$, K$_2$SO$_{4(s)}$,
592  KHSO$_{4(s)}$, KNO$_{3(s)}$, KCl$_{(s)}$, MgSO$_{4(s)}$, Mg(NO$_3$)$_{2\ (s)}$, MgCl$_{2(s)}$, H$^+_{(aq)}$, Na$^+_{(aq)}$, NH$_4^+_{(aq)}$, Cl$^-_{(aq)}$, NO$_3^-_{(aq)}$, SO$_4^{2-}_{(aq)}$, HSO$_4^-_{(aq)}$, Ca$^{2+}_{(aq)}$,
593  K$^+_{(aq)}$ and Mg$^{2+}_{(aq)}$) (Table S4 and Figure S10). Overall, the components were negatively correlated with RH and positively
594  with temperature, indicating dry air masses and unfavorable conditions for the dispersion of atmospheric pollutants (Sánchez-
595  Ccoyllo et al., 2002). More discussions are presented in the SI.
596      The biomass burning (BB) factor correlated with BPe and InP, species typically associated with vehicular emissions
597  (Ravindra et al., 2008). However, the InP/(BPe+InP) polar plots suggested an influence of biomass burning with northwest
598  strong winds (Sect. 3.2). The low correlation of retene with BB and levoglucosan suggests that this species may be related to
599  a local biomass burning source or the influence of gas-particle partition of this semi-volatile species (Ravindra et al., 2008).
600  Chloride was moderately correlated with BB and VE2 factors (r > 0.5), strongly correlated with mannosan and EC1 (r > 0.7),
601  and weakly correlated with levoglucosan. This suggests a different biomass burning profile, such as wood burning in
602  restaurants or biomass burning associated with waste (Kumar et al., 2015). Xylitol was weakly correlated with BB and VE1 (r
603  > 0.3). It also presented a moderate negative correlation with RH (r ~ -0.3), suggesting an increase under drier conditions.

Notably, it presented weaker correlations with potassium compared to Lev, suggesting a biomass burning origin that is less associated with crop burning. The association of xylitol with biomass burning was observed in other studies (Clemente et al., 2024; Gonçalves et al., 2021).

The secondary aerosol formation (SF) factor was moderately correlated with the modeled liquid inorganic aerosol and water content of the aerosol, and the modeled secondary species $NH_4^+{}_{(aq)}$, $SO_4^{2-}{}_{(aq)}$, and $HSO_4^-{}_{(aq)}$ (r > 0.6). Correlation with modeled water content suggests that the secondary formation pathway in São Paulo depends on humidity. $SO_4^{2-}$ and $NO_3^-$ formation in clouds and fog droplets were attributed mainly to the heterogeneous aqueous transformation of $SO_2$ and $NO_x$ under high relative humidity (RH) during haze episodes in Beijing (Huang et al., 2016). Sulfate particles can grow in the aerosol droplet process (Guo et al., 2010). Among the ratios, the SF factor presented weak to moderate correlations with $NO_3^-$/EC, $SO_4^{2-}$/EC, and $NO_3^-$/Zn (r > 0.4), suggesting that they can help identify secondary formation events, an opposite trend to that observed for the BB, VE1, and VE2 factors.

The industrial (IN) factor presented moderate correlations with the liquid inorganic aerosol and water content in the aerosol, possibly associated with more humid air masses from the east observed in the polar plot, as particles can grow in the aerosol droplet process (Guo et al., 2010). Notably, it was correlated with aerosol acidity ($H^+{}_{(aq)}$), perhaps due to simultaneous emission of gaseous oxides that can undergo secondary reactions and produce acidic species. $H^+{}_{(aq)}$ was also moderately correlated with nitrate, suggesting an influence of nitric acid (Ianniello et al., 2011). Selenium, previously attributed to industrial sources in the MASP (Vieira et al., 2023), was moderately associated with the IN factor. Sn was moderately correlated with IN (r ~0.5) and strongly correlated with Tl. The IN factor presented a weak correlation with the V/Ni ratio (r~0.5), denoting the contribution from the burning of crude oil (Johnson et al., 2014). IN was also moderately correlated with $NO_3^-$/EC, suggesting a connection with secondary formation. There was a weak correlation between SF and IN, pointing to a common origin between both, maybe due to the emission of gaseous precursors and secondary formation.

The PMF factor associated with vehicular exhaust and dust resuspension (VE1) presented weak correlations with most species. The factor presented moderate correlations with the modeled mass of solid inorganic aerosol (r ~ 0.6). This factor also displayed a moderate positive correlation with temperature (r > 0.6) and negative with relative humidity and pressure (r < -0.5), suggesting an increase of this factor during prefrontal conditions.

The local vehicular source (VE2) presented higher correlations with BaA and HMW-PAHs such as Per, InP, BPe, and Cor (r > 0.5), which are found in LDV emissions (Pereira et al., 2023a). Among the identified factors, VE2 and BB presented higher correlations with the toxicity equivalent indexes BaP-TEQ and BaP-MEQ (r > 0.5), suggesting a contribution of these sources to potential carcinogenicity and mutagenicity. La was moderately associated with VE2 and strongly with Mn, Co, and Ce. La and Ce derive mainly from catalyst emissions (Kulkarni et al., 2006). Fe presented strong correlations with VE2, Ti, Mn, and Ce. These species are linked to vehicular and soil-related sources (Pereira et al., 2017a, Brito et al., 2013). Cobalt, a component of tire debris (Thorpe and Harrison, 2008), was moderately correlated with VE2 and strongly correlated with La, Tl, and Mn. VE2 presented moderate correlations with Fe/$Ca^{2+}$ (r ~0.6), which may indicate enrichment of anthropogenic iron (Pereira et al., 2023a).

Some species were less specific to particular sources. $PO_4^{3-}$ presented no correlations with PMF factors and was moderately correlated with $Na^+$ and $Ca^{2+}$ (r > 0.45). Oxalate was not correlated with specific factors. It presented moderate correlations with $NH_4^+$, $K^+$, $NO_3^-$, $SO_4^{2-}$, As, Rb, Sb, Tl, Pb, and OC (r > 0.5). This suggests multiple sources for oxalate, as previously observed, such as vehicle exhaust, biomass burning, and biogenic activity, and secondary formation (Guo et al., 2010). $Na^+$ was not specific for any source, as previously observed in the MASP (Vieira-Filho et al., 2016b). This species presented a weak correlation with some other species ($Ca^{2+}$, $Cl^-$, $PO_4^{3-}$, As, Rb, Sr, and Cd) (r > 0.3). The lack of strong correlation with $Cl^-$ can be explained by the relatively low influence of sea spray in the studied period as indicated by the trajectories (Section 3.1). Aluminum displayed low correlations with the PMF factors and was strongly correlated with Ti (r > 0.7) and moderately with Ce (r > 0.6), pointing to its origin in crustal materials (Hetem and Andrade, 2016). Ti was also

strongly correlated with Ce. Both species presented low enrichment (Section 3.6), suggesting a mineral origin apart from vehicular emissions. Chromium was not correlated to PMF factors but presented a relatively high correlation with Ni (r ~0.5). Both species were previously associated with industrial sources (Bourotte et al., 2011; Castanho and Artaxo, 2001). Arsenic, a highly toxic element, showed relatively moderate correlations with BB, IN, and VE2 and strong with Rb, Ag, and Cd. Arsenic has multiple sources, including industries (Calvo et al., 2013).

### 3.5 Particle size distributions: associations with aerosol source apportionment and meteorological scenarios

Submicrometer particle number size distributions monitoring provided information about the relative contribution of different particle size modes and their temporal evolution. Total particle number concentrations averaged $1.03 \pm 0.59 \ 10^4 \ cm^{-3}$, with a mean geometric diameter of $51 \pm 16.1$ nm. Size distributions were dominated by the Aitken mode (mean geometric diameter range 50-100 nm) and the accumulation mode (diameter above 100 nm), respectively, accounting for 46% and 32% of particle number concentrations, on average. The nucleation mode (mean geometric diameter below 30 nm) was less frequent, contributing to an average of 21% of the particle number concentration, on average (Table S5). Events of new particle formation and growth were infrequent, possibly due to the relatively high particle loading and condensational sink. Nearly 70% of the monitored particles had diameters below 100 nm, classified as ultrafine particles, which can penetrate the extensive area of the lungs and reach other organs through the lung vasculature (Schraufnagel, 2020). The predominance of Aitken mode particles suggests the influence of relatively fresh particles compared to the typically aged accumulation mode particles. A previous study in the MASP reported associations between inorganic species and the Aitken mode particles, whereas aged oxygenated organic particles were mainly associated with the accumulation mode (Monteiro dos Santos et al., 2021).

The size distribution measurements were averaged to match the filter sampling periods, providing a link with the aerosol chemical composition measurements and source apportionment. No significant differences were observed in the particle size distributions in days with a predominance of vehicular emissions or biomass burning. Although the aerosol chemical composition differed under the influence of different emission sources (Section 3.3), the particle size distributions were typically dominated by the Aitken mode, suggesting the presence of relatively fresh particles. However, there was a clear difference in the size distributions measured under high aerosol loadings ($PM_{2.5} \geq 15 \ \mu g \ m^{-3}$, WHO guideline), with an increase of Aitken and accumulation mode particles, especially at the end of the day (Figure S11). The atmospheric conditions associated with high PM concentration (low boundary layer height, weak ventilation, absence of precipitation, and clear sky conditions) likely favored secondary aerosol production and particle growth by condensation in pre-existing particles (Sánchez-Ccoyllo and Andrade, 2002; Santos et al., 2018), which might explain the increase of larger particles (Monteiro dos Santos et al., 2021).

Four days were selected within the study period to assess the dynamics of particle size distribution in high temporal resolution and the influence of different meteorological scenarios. Figures 9a and 9b show the evolution of size distributions in two days with a strong contribution of secondary aerosol formation, according to the source apportionment analysis (Figure 7). New particle formation events were observed these days, with sub-30 nm particles emerging in the morning, followed by a consistent growth towards the Aitken mode until the mid-afternoon, with growth rates of 5.1 and 3.3 nm h$^{-1}$, respectively. The observed growth may be associated with the condensation of secondary organic and inorganic aerosol species. Previous studies in São Paulo indicated a large fraction of secondary inorganic species in the Aitken mode, likely produced from the reaction of nitric acid and ammonia (Carbone et al., 2013; Monteiro dos Santos et al., 2021). Another interesting feature was the entrance of the sea breeze around 4 PM local time on August 15, marked by a dashed line in Figure 9a. The sea breeze affected the measured size distributions, leading to a fast particle concentration decrease, from $1.8 \ 10^4$ to $1.0 \ 10^4 \ cm^{-3}$, associated with a mean geometric diameter increase from $44.2 \pm 2.0$ to $47.0 \pm 2.0$ nm. The observed changes in the size

688  distribution may be explained by the transport of cleaner and humid air from the coast. In addition to oceanic air masses, aged

689  particles from industrial emissions near the coast may also be transported to the MASP during sea breeze events.
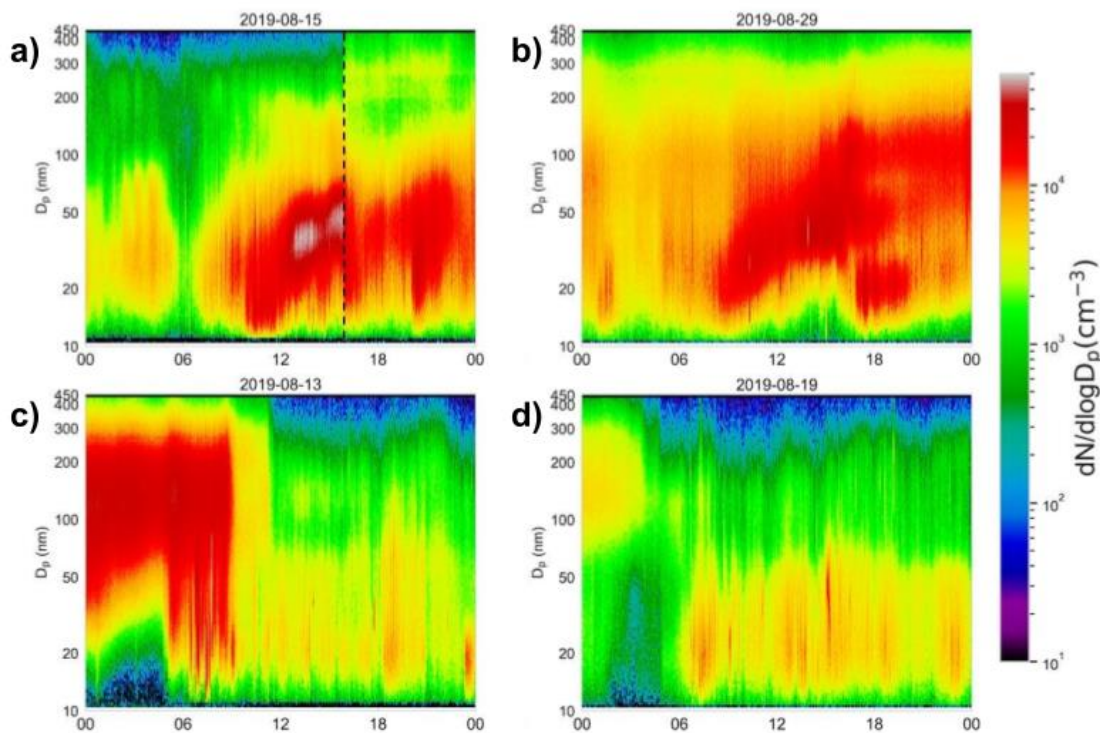
691  **Figure 9:** Submicrometer particle number size distributions for **(a)** August 15, **(b)** 29 , **(c)** 13 , and **(d)** 19. The x-axis

692  represents the timeline (local time), the y-axis refers to particle diameters, and the colors represent the number of particles

693  normalized by diameter bins.

694  On the other hand, Figures 9c and 9d show examples of the influence of cold fronts on particle size distributions. The

695  prefrontal period is typically characterized by stagnant atmospheric conditions that favor the occurrence of high $PM_{2.5}$

696  concentrations. The emergence of the cold front on the morning of August 19 resulted in increased ventilation and precipitation

697  (Figure S12), leading to a strong decrease in the particle number concentrations, from $2.8 \ 10^4$ to $0.5 \ 10^4$ cm$^{-3}$. A decrease in

698  the geometric mean diameter was simultaneously observed, from $94.7 \pm 2.0$ to $43.8 \pm 2.0$ nm, indicating that the particle

699  removal by rain and winds was more efficient for accumulation mode particles. Figure 9 provides examples of sub-daily

700  variability in aerosol properties, which cannot be discerned in the aerosol filter samples.

701  **3.6**     **Chemical and source characteristics of pollution event days**

702  The sampling days were separated between high pollution days (with $PM_{2.5}$ above the WHO guideline of 15 μg m$^{-3}$) and low

703  pollution days (below). These polluted periods were associated with relatively higher average temperatures and lower humidity

704  (19 ℃ and 74%, compared to 15 ℃ and 83%). During these pollution events, $PM_{2.5}$ increased by 171%, and carbonaceous

705  species (OM+EC) represented a higher mass fraction (nearly 60%) (Figure 10). In polluted periods, the accumulation processes

706  can lead to the formation of organic coatings on black carbon particles (Monteiro dos Santos et al., 2021). On the other hand,

707  oxides, other WSI, and sulfate accounted for a higher fraction in non-event days. The unidentified fraction, attributed to

708  unmeasured components such as carbonate or water (Pereira et al., 2017a), was also slightly higher in non-event days. In

709  absolute numbers, all PMF factors increased on event days. However, the BB factor contribution increased significantly on

710  polluted days, rising from 4 to 27% of the $PM_{2.5}$ mass.

711
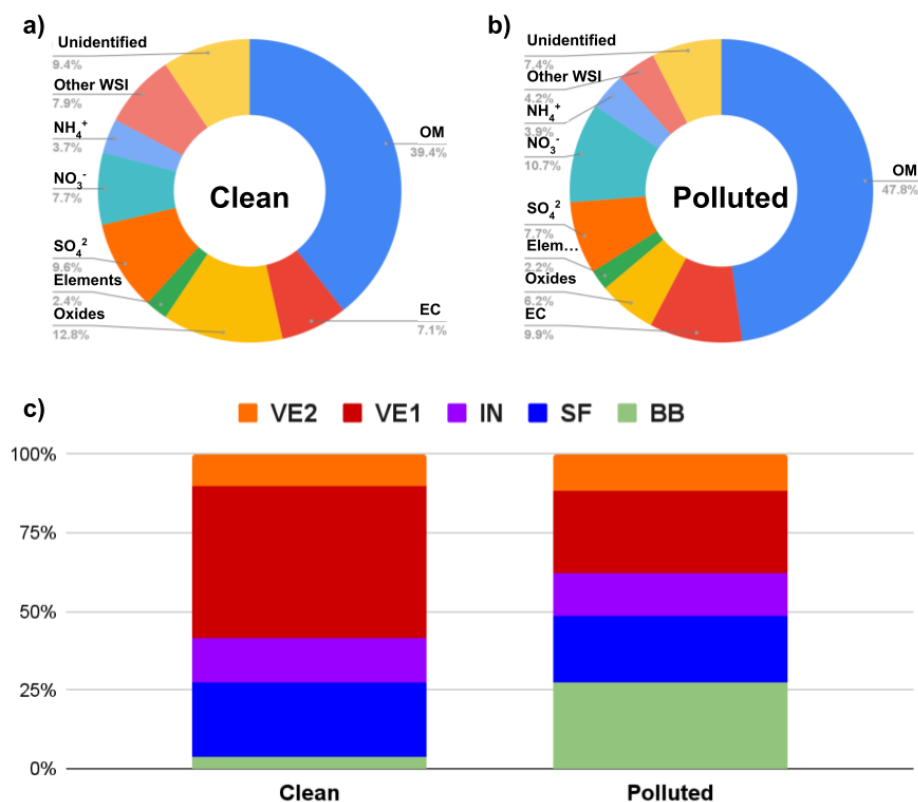
712 **Figure 10:** Chemical mass balance for clean (PM$_{2.5}$ < 15 μg m$^{-3}$) **(a)** and polluted days (PM$_{2.5}$ ≥ 15 μg m$^{-3}$) **(b)**, and

713 PMF source contributions for both periods **(c).**

714

715      OC, EC, K$^+$, NO$_3^-$, V, Mn, Fe, Co, Zn, Rb, Cd, Sn, Sb, Ce, Tl, Pb, and Lev presented a significantly higher increase

716 than that observed for PM$_{2.5}$ in these polluted periods (Table S6 and Figure S13), suggesting an accumulation of these species

717 during these events ($p < 0.05$). In percentage terms, all OC and EC fractions increased more than PM$_{2.5}$ ($p < 0.05$), except OC1,

718 EC3, and EC4. Proportionally, retene increased less than PM$_{2.5}$, suggesting that it may be linked to a local biomass-burning

719 source, such as wood burning in restaurants (Andrade et al., 2017; Kumar et al., 2016). Mannosan followed the same trend.

720 The toxicity indexes BaP-TEQ and BaP-MEQ presented significant increases ($p < 0.05$), caused mainly by the rise in HMW-

721 PAHs due to the accumulation of fossil-fuel and biomass burning emitted aerosols (Vasconcellos et al., 2010). Furthermore,

722 there seems to be an accumulation of other toxic species from anthropogenic sources, such as potentially toxic elements (PTE)

723 such as Cd, Sb, and Pb (Pereira et al., 2023b; Thorpe and Harrison, 2008). However, the toxicity unity (TU) did not increase

724 as much (~50%). Phosphate was the only species to decrease, although with $p > 0.05$. It is often associated with dust and

725 farming activities (Yuan et al., 2008; Allen et al., 2010). In the present study, the most probable source was the soil.

726      Levoglucosan concentration tripled during the polluted days (423 and 140 ng m$^{-3}$, respectively). Ionic potassium

727 quadrupled these days (330 and 82 ng m$^{-3}$), suggesting a higher impact of crop and other types of biomass burning (Chow et

728 al., 2022a). However, levoglucosan represented similar portions of OM on both occasions (nearly 3%). Xylitol and mannosan

729 presented a lower increase on polluted days ($p < 0.05$), suggesting they are associated with other types of biomass burning. In

730 2020, it was observed that during smoke plume events in the MASP, PM$_{2.5}$ surpassed 25 μg m$^{-3}$ at 99% of the air quality

731 monitoring stations. These days, the plumes were mainly associated with sugarcane burning and often with the contribution of

732 wildfires in the Amazon and Pantanal biomes (Souto-Oliveira et al., 2023). In that study, the authors were able to differentiate

733 CO$_2$ from local wood burning (4-7%) from that from remote forest wildfires (4-26%). In recent years, the influence of remote

734 forest burning has occurred, likely related to natural seasonal variations and climate change, with lower humidity and

735 precipitation and increased fires (Goss et al., 2020; Abram et al., 2021). The influence of biomass burning in the metropolitan

area often occurs above the boundary layer. However, these plumes from remote regions can still influence the concentration and composition of PM$_{2.5}$ at the surface (Souto-Oliveira et al., 2023).

Enrichment factors for the elements were above 10 for Cr, Cu, Zn, As, Se, Mo, Ag, Cd, Sn, Sb, Ba, Tl, Pb, Bi, and U (Figure 11), suggesting a strong anthropogenic character. Overall, there was an increase in the enrichment factors of metals in the polluted period, five times higher for Fe and similar for U, suggesting that these are mostly soil-bound in the clean period. Despite the very low concentrations, Se, Sb, and Bi presented the highest EFs (near and above 10,000), indicating a very high anthropogenic character. Selenium was previously attributed to anthropogenic sources such as fossil fuel combustion, waste burning, tires and paper, coal combustion, oil, and glass industries (Mehdi et al., 2013). Additionally, it was previously attributed to industrial sources in the eastern part of the MASP (Vieira et al., 2023). Antimony is associated with non-exhaust emissions (brake wear) (Thorpe and Harrison, 2008) and non-ferrous metal industries (Calvo et al., 2013). Bismuth is related to anthropogenic sources, such as fossil fuel combustion, metallurgy, and refuse incineration (Ferrari et al., 2000). Other species presented low EFs, attributed to geogenic sources: Ti, Fe, and Co (EFs near and below 1). Often associated with catalyst emissions (Kulkarni et al., 2006), La and Ce displayed relatively low enrichment factors (below 5). Some species exhibited a geogenic character in the clean periods and a more anthropogenic character in the polluted period, with K, V, Ni, and Rb approaching an EF of 10.
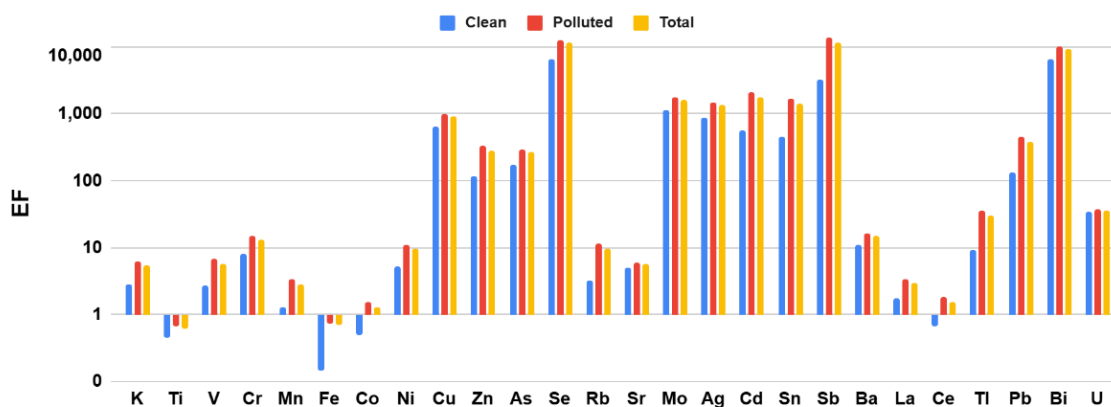
**Figure 11:** Enrichment factors (EF) for the clean, polluted, and total period.

### 3.7    Ecotoxicity assays

Ecotoxicity tests of aqueous particulate matter extracts were performed with the bacteria *Aliivibrio fisheri*. All samples in this study were classified as toxic, with toxic unity (TU) values ranging from 1.7 to 7.1, averaging 3.7. The highest values were obtained in periods impacted by biomass burning (Figure S14). The TU unit showed moderate correlations with levoglucosan, water-soluble K$^+$, and the modeled aqueous K$^+$ (r > 0.5), which may be associated with biomass burning aerosols and water-soluble organic species (not quantified in the study) (Urban et al., 2012). Among the factors obtained by receptor modeling, biomass burning had the highest correlation with TU (Table S5), indicating that water-soluble components trigger the toxicity of particles emitted by this source. The vehicular-exhaust factor exhibited the second highest correlation with TU, although weak. In addition, the TU values presented moderate correlations with elements known to be toxic and associated with vehicular sources such as Pb (r ~ 0.5). The correlation was moderate (r > 0.5) with OC (higher for fractions OC2, OC3, and OC4, less volatile and more oxidized) and EC (higher for fractions EC1 and EC2). Significant correlations between the bioluminescence inhibition responses and the contributions of biomass burning and traffic to particulate matter concentrations were also reported for Coimbra, Portugal (Alves et al., 2021). As observed in the present study, toxicity was statistically correlated with OC, EC, anhydrosugars, and elements from exhaust and non-exhaust emissions. Since biomass burning and traffic emissions may elicit acute toxic effects, adopting source-specific preventive and remedial measures is necessary.

## 4 Summary and conclusions

Fine particulate matter (PM$_{2.5}$) was collected in a 100-day dry period in 2019, covering the period from June to early September, when several pollution events were observed, surpassing the WHO daily limit of 15 μg m$^{-3}$ in 75% of the days. Chemical characterization was obtained, including water-soluble ions, elements, carbonaceous species, anhydrosugars, and polycyclic aromatic hydrocarbons. Additionally, the size distribution of particles (SMPS) was monitored simultaneously. PM$_{2.5}$ levels were, however, lower than in previous studies. The lower sulfate-to-nitrate ratios suggested a decrease in sulfur oxide levels. A higher contribution of organic matter to particulate matter indicated an increase in the secondary formation of organic species and a reduction of elemental carbon emissions by vehicles. However, a further study should be performed to statistically assess this trend over the last decades. The impact of oxidant atmosphere and higher temperatures on the formation of secondary organic carbon and the effect of industrial emissions on sulfate production require further investigation.

As for biomass burning, typically observed in the dry period, there was a decrease in the contribution of sugarcane straw burning since there was a change in the K$^+$/Lev and Lev/Man ratios and relatively lower potassium levels. However, the long-range transport of plumes from forest fires and agricultural burning in regions north and northwest of MASP remains a significant source of PM$_{2.5}$ in this period, as the average concentration of levoglucosan remained high. Other authors have observed a further increase in the influence of bagasse-burning plants and the intrusion of aerosols from forest fires originating in central and northern Brazil. This last phenomenon is related to climate change and has increased in the last decades (longer dry periods). The increase in the Lev/Man ratio with stronger winds suggests the contribution of different types of biomasses. Correlations with other species and the PMF receptor model suggested Rb as a reliable biomass-burning tracer. PAHs remain a concern due to increasing concentrations and equivalent toxicity values exceeding 1 ng m$^{-3}$ in half of the samples. However, the levels are lower than those observed in previous studies. The vehicular-related species BbF remained an abundant PAH, suggesting it is a persistent constituent. Furthermore, PAH diagnostic ratios fell within the range observed for vehicular emissions. The increased concentrations of these pollutants are likely related to the lower dispersion in this season. Additionally, increasing V/Ni and La/Ce ratios with east and southeast winds suggested a contribution of aerosols from petrochemical industrial areas, which can occur with meteorological conditions characterized by cold fronts and sea breezes.

The PMF receptor model was applied to assess the PM$_{2.5}$ sources, and a five-factor solution was obtained (biomass burning, secondary formation, industrial, vehicular+road dust, and local vehicular). A high contribution of biomass burning, associated with north and northwest winds, was observed, reaching one-fourth of the particulate matter. Considering the previous source apportionment studies, sources related to vehicular emissions are still dominant (40% of PM$_{2.5}$). A mixed factor of road dust and vehicular emissions increased throughout the campaign, suggesting a more significant influence of resuspension at the end of the winter. Relatively lower, an industrial contribution was observed, increasing with northeast winds that pass through industrial areas of MASP. The PMF solution showed overlapping contributions in some factors, which may be related to the low temporal resolution of sampling and the fact that emissions from various sources mix before reaching the semi-background receptor site. Enhancing the time resolution in future investigations may help identify more sources.

Two particle formation events were identified by SMPS in days with pronounced secondary formation and happened before the arrival of the sea breeze. The sulfate secondary formation was related to humid conditions, as suggested by correlations between the contribution of secondary formation and the aerosol's modeled water content (ISORROPIA). During days of pollution events (PM$_{2.5}$ > 15 μg m$^{-3}$), carbonaceous species represented a higher fraction of particulate matter, while sulfate's contribution was reduced. An accumulation of PAHs and toxic species such as Cd, Sb, and Pb on these days represents a health concern. These pollution events were associated with a relative increase in the contribution of the biomass burning factor, whose emissions, added to pollutants emitted and formed locally, contribute to the degradation of air quality in the dry season. Throughout the sampling campaign, all samples were classified as ecotoxic. The ecotoxicity correlated with the biomass burning factor, highlighting the importance of regulating this source for air quality control. These results indicate that

810 controlling PM$_{2.5}$ exceedance events should include regulating emerging biomass burning sources and stricter rules concerning
811 vehicular emissions.
812

813 **Data availability**
814 The datasets will be available upon request after publishing.
815

816 **Author contributions**
817 GMP performed part of the analyses (OC, EC, elements, and water-soluble ions), the data treatment and led the manuscript
818 writing. MFA managed the project, provided infrastructure, designed the study and revised the manuscript. PCV provided
819 infrastructure, designed the study and revised the manuscript. LYK performed the data treatment. RFB monitored the particle
820 size distribution and contributed with the writing. DMS helped with the OC and EC determination and revised the manuscript.
821 TSS performed the PAHs extraction and characterization. CG characterized the anhydrosugars. ICR performed the ecotoxicity
822 essays and helped with the revisions. CA, NK, LR, PA, and EDF provided infrastructure and revised the manuscript. TN,
823 RMM, and MAY revised the paper.
824

825 **Competing interests**
826 The authors declare that they have no conflict of interest.
827

828 **Acknowledgements**

829 These results were part of the "Chemical and toxicological SOurce PROfiling" of particulate matter in urban air project
830 (SOPRO, Grant no. POCI-01-0145-FEDER-029574), supported by the Portuguese Foundation for Science and Technology
831 from the Ministry of Science, Technology, and Higher Education (FCT/MCTES), and by the São Paulo Research Foundation
832 (FAPESP; Grant #2018/07848-9). SOPRO project was also funded by FEDER, through COMPETE2020—Programa
833 Operacional Competitividade e Internacionalização (POCI), and by national funds (OE), through FCT/MCTES. The authors
834 also acknowledge FAPESP for Grants #2016/18438-0 (Metroclima project, for research resources) and #2019/01316-8
835 (URBESP project, scholarship), and National Research Council for the grants (CNPq 301503/2018-4). The financial support
836 to CESAM by FCT/MCTES (UIDP/50017/2020 + UIDB/50017/2020 + LA/P/0094/2020), through national funds, is also
837 acknowledged. Meteorological data (irradiance, atmospheric pressure, temperature and relative humidity) were kindly
838 provided by the IAG-USP meteorological station and the Climatology and Biogeography Laboratory (Department of
839 Geography - FFLCH - USP).

840 **References**

841 Abram, N.J., Henley, B.J., Sen Gupta, A., Lippmann, T.J.R., Clarke, H., Dowdy, A.J., Sharples, J.J., Nolan, R.H., Zhang, T.,
842 Wooster, M.J., Wurtzel, J.B., Meissner, K.J., Pitman, A.J., Ukkola, A.M., Murphy, B.P., Tapper, N.J., Boer, M.M.:
843 Connections of climate change and variability to large and extreme forest fires in southeast Australia, Commun. Earth Environ.,
844 2, 1-17, https://doi.org/10.1038/s43247-020-00065-8, 2021.

845 de Abrantes, R., Vicente de Assunção, J., Pesquero, C. R., Bruns, R. E. and Nóbrega, R. P.: Emission of polycyclic aromatic
846 hydrocarbons from gasohol and ethanol vehicles, Atmos. Environ., 43(3), 648–654,
847 https://doi.org/10.1016/j.atmosenv.2008.10.014, 2009.

848 Akyüz, M. and Cabuk, H.: Gas-particle partitioning and seasonal variation of polycyclic aromatic hydrocarbons in the
849 atmosphere of Zonguldak, Turkey., Sci. Total Environ., 408(22), 5550–5558, https://doi.org/10.1016/j.scitotenv.2010.07.063,
850 2010.

851 Allen, A.G., Cardoso, A.A., Wiatr, A.G., Machado, C.M.D., Paterlini, W.C., and Baker, J.: Influence of intensive agriculture
852 on dry deposition of aerosol nutrients, J. Braz. Chem. Soc., 21, 1, https://doi.org/10.1590/S0103-50532010000100014, 2010.

Almeida, S. M., Pio, C. A., Freitas, M. C., Reis, M. A. and Trancoso, M. A.: Approaching PM$_{2.5}$ and PM$_{2.5\text{-}10}$ source apportionment by mass balance analysis, principal component analysis and particle size distribution., Sci. Total Environ., 368(2–3), 663–674, https://doi.org/10.1016/j.scitotenv.2006.03.031, 2006.

Alves, C., Rienda, I. C., Vicente, A., Vicente, E., Gonçalves, C., Candeias, C., Rocha, F., Lucarelli, F., Pazzi, G., Kováts, N., Hubai, K., Pio, C. and Tchepel, O.: Morphological properties, chemical composition, cancer risks and toxicological potential of airborne particles from traffic and urban background sites, Atmos. Res., 264, 105837, https://doi.org/10.1016/j.atmosres.2021.105837, 2021.

Alves, C. A., Evtyugina, M., Vicente, A. M. P., Vicente, E. D., Nunes, T. V., Silva, P. M. A., Duarte, M. A. C., Pio, C. A., Amato, F. and Querol, X.: Chemical profiling of PM$_{10}$ from urban road dust., Sci. Total Environ., 634, 41–51, https://doi.org/10.1016/j.scitotenv.2018.03.338, 2018.

Alves, C. A., Vicente, A. M. P., Calvo, A. I., Baumgardner, D., Amato, F., Querol, X., Pio, C. and Gustafsson, M.: Physical and chemical properties of non-exhaust particles generated from wear between pavements and tyres, Atmos. Environ., 224, 117252, https://doi.org/10.1016/j.atmosenv.2019.117252, 2020.

Amarillo, A. C. and Carreras, H.: Quantifying the influence of meteorological variables on particle-bound PAHs in urban environments, Atmos. Pollut. Res., 7(4), 597–602, https://doi.org/10.1016/j.apr.2016.02.006, 2016.

Amato, F., Alastuey, A., Karanasiou, A., Lucarelli, F., Nava, S., Calzolai, G., Severi, M., Becagli, S., Gianelle, V. L., Colombi, C., Alves, C., Custódio, D., Nunes, T., Cerqueira, M., Pio, C., Eleftheriadis, K., Diapouli, E., Reche, C., Minguillón, M. C., Manousakas, M.-I. and Querol, X.: AIRUSE-LIFE+: a harmonized PM speciation and source apportionment in five southern European cities, Atmospheric Chemistry and Physics, 16(5), 3289–3309, https://doi.org/10.5194/acp-16-3289-2016, 2016.

Andrade, F., Orsini, C. and Maenhaut, W.: Relation between aerosol sources and meteorological parameters for inhalable atmospheric particles in Sao Paulo City, Brazil, Atmos. Environ., 28(14), 2307–2315, https://doi.org/10.1016/1352-2310(94)90484-7, 1994.

Andrade, M.F., Kumar, P., de Freitas, E. D., Ynoue, R. Y., Martins, J., Martins, L. D., Nogueira, T., Perez-Martinez, P., de Miranda, R. M., Albuquerque, T., Gonçalves, F. L. T., Oyama, B. and Zhang, Y.: Air quality in the megacity of São Paulo: Evolution over the last 30 years and future perspectives, Atmos. Environ., 159, 66–82, https://doi.org/10.1016/j.atmosenv.2017.03.051, 2017.

Andrade, M.F., de Miranda, R.M., Fornaro, A., Kerr, A., Oyama, B., de Andre, P.A., Saldiva, P. Vehicle emissions and PM$_{2.5}$ mass concentrations in six Brazilian cities. Air Qual. Atmos. Health, 5, 79-88, https://doi.org/10.1007/s11869-010-0104-5 , 2012.

Artaxo, P., Gerab, F., Yamasoe, M. A. and Martins, J. V.: Fine mode aerosol composition at three long-term atmospheric monitoring sites in the Amazon Basin, J. Geophys. Res., 99(D11), 22857, https://doi.org/10.1029/94JD01023, 1994.

Aubin, S. and Farant, J. P.: Benzo[b]fluoranthene, a potential alternative to benzo[a]pyrene as an indicator of exposure to airborne PAHs in the vicinity of Söderberg aluminum smelters., J. Air Waste Manag. Assoc., 50(12), 2093–2101, https://doi.org/10.1080/10473289.2000.10464236, 2000.

Bhattarai, H., Saikawa, E., Wan, X., Zhu, H., Ram, K., Gao, S., Kang, S., Zhang, Q., Zhang, Y., Wu, G., Wang, X., Kawamura, K., Fu, P. and Cong, Z.: Levoglucosan as a tracer of biomass burning: Recent progress and perspectives, Atmos. Res., 220, 20–33, https://doi.org/10.1016/j.atmosres.2019.01.004, 2019.

Bian, Y. X., Zhao, C. S., Ma, N., Chen, J. and Xu, W. Y.: A study of aerosol liquid water content based on hygroscopicity measurements at high relative humidity in the North China Plain, Atmospheric Chemistry and Physics, 14(12), 6417–6426, https://doi.org/10.5194/acp-14-6417-2014, 2014.

Bourotte, C., Forti, M. C., Melfi, A. J. and Lucas, Y.: Morphology and solutes content of atmospheric particles in an urban and a natural area of São Paulo state, Brazil, Water Air Soil Pollut., 170(1–4), 301–316, https://doi.org/10.1007/s11270-005-9001-1, 2006.

Bourotte, C. L. M., Sanchéz-Ccoyllo, O. R., Forti, M. C. and Melfi, A. J.: Chemical composition of atmospheric particulate matter soluble fraction and meteorological variables in São Paulo state, Brazil, Rev. bras. meteorol., 26(3), 419–432, https://doi.org/10.1590/S0102-77862011000300008, 2011.

Brito, J., Rizzo, L. V., Herckes, P., Vasconcellos, P. C., Caumo, S. E. S., Fornaro, A., Ynoue, R. Y., Artaxo, P. and Andrade, M. F.: Physical–chemical characterisation of the particulate matter inside two road tunnels in the São Paulo Metropolitan Area, Atmospheric Chemistry and Physics, 13(24), 12199–12213, https://doi.org/10.5194/acp-13-12199-2013, 2013.

Brito, J., Carbone, S., A. Monteiro dos Santos, D., Dominutti, P., de Oliveira Alves, N., Rizzo, L. V., Artaxo, P.: Disentangling vehicular emission impact on urban air pollution using ethanol as a tracer. Scientific Reports, 8, 10679, https://doi.org/10.1038/s41598-018-29138-7, 2018.

Buchholz, R.R., Park, M., Worden, H.M., Tang, W., Edwards, D.P., Gaubert, B., Deeter, M.N., Sullivan, T., Ru, M., Chin, M., Levy, R.C., Zheng, B., Magzamen, S.: New seasonal pattern of pollution emerges from changing North American wildfires. Nat Commun 13, 2043. https://doi.org/10.1038/s41467-022-29623-8, 2022.

Calvo, A. I., Alves, C., Castro, A., Pont, V., Vicente, A. M. and Fraile, R.: Research on aerosol sources and chemical composition: Past, current and emerging issues, Atmos. Res., 120–121, 1–28, https://doi.org/10.1016/j.atmosres.2012.09.021, 2013.

Carbone, S., Saarikoski, S., Frey, A., Reyes, F., Reyes, P., Castillo, M., Gramsch, E., Oyola, P., Jayne, J., Worsnop, D. R. and Hillamo, R.: Chemical characterization of submicron aerosol particles in Santiago de Chile, Aerosol Air Qual. Res., 13(2), 462–473, https://doi.org/10.4209/aaqr.2012.10.0261, 2013.

Carvalho, J.S., do Nascimento, R.K.S., J Cintra, J.V.F.R.F., da Rosa, N.L.C., Grosseli, G.M., Fadini, P.S., Urban, R.C.: Source apportionment and health impact assessment of atmospheric particulate matter in the city of São Carlos, Brazil, Chemosphere, 326, 138450, https://doi.org/10.1016/j.chemosphere.2023.138450, 2023.

Caseiro, A., Marr, I.L., Claeys, M., Kasper-Giebl, A., Puxbaum, H., Pio, C.: Determination of saccharides in atmospheric aerosol using anion-exchange high-performance liquid chromatography and pulsed-amperometric detection, J. Chromatogr. A, 1171, 37-45, https://doi.org/10.1016/j.chroma.2007.09.038, 2007.

Caseiro, A., Bauer, H., Schmidl, C., Pio, C. A. and Puxbaum, H.: Wood burning impact on $PM_{10}$ in three Austrian regions, Atmos. Environ., 43(13), 2186–2195, https://doi.org/10.1016/j.atmosenv.2009.01.012, 2009.

Castanho, A. D. A. and Artaxo, P.: Wintertime and summertime São Paulo aerosol source apportionment study, Atmos. Environ., 35(29), 4889–4902, https://doi.org/10.1016/S1352-2310(01)00357-0, 2001.

Caumo, S., Traub, A., Evans, G. and de Castro Vasconcellos, P.: Health risk assessment in atmosphere near a petrochemical industrial complex: Measuring oxidative potential and oxidative burden, Atmos. Pollut. Res., 13(7), 101457, https://doi.org/10.1016/j.apr.2022.101457, 2022.

Cavalli, F., Viana, M., Yttri, K. E., Genberg, J. and Putaud, J. P.: Toward a standardised thermal-optical protocol for measuring atmospheric organic and elemental carbon: the EUSAAR protocol, Atmos. Meas. Tech., 3(1), 79–89, https://doi.org/10.5194/amt-3-79-2010, 2010.

Cecinato, A.: Polynuclear aromatic hydrocarbons (PAH), benz(a)pyrene (BaPY) and nitrated-PAH (NPAH) in suspended particulate matter. Ann Chim 87, 483–496, 1997.

CETESB: Companhia de Tecnologia do Saneamento Ambiental: Relatório de qualidade do ar no Estado de São Paulo 2014, Report of air quality in the São Paulo State 2014, São Paulo, Brazil, available at: http://ar.cetesb.sp.gov.br/ publicacoes-relatorios/ (last access: 1 February 2024), 2015.

CETESB: Companhia de Tecnologia do Saneamento Ambiental: Relatório de qualidade do ar no Estado de São Paulo 2019, Report of air quality in the São Paulo State 2019, São Paulo, Brazil, available at: http://ar.cetesb.sp.gov.br/publicacoes-relatorios/, 2020.

CETESB: Companhia de Tecnologia do Saneamento Ambiental: Relatório de qualidade do ar no Estado de São Paulo 2022, Report of air quality in the São Paulo State 2022, São Paulo, Brazil, available at: http://ar.cetesb.sp.gov.br/publicacoes-relatorios/ (last access: 1 February 2024), 2023.

CETESB: Proconve – Programa de Controle da Poluição do Ar por Veículos Automotores - Companhia Ambiental do Estado de São Paulo, https://cetesb.sp.gov.br/veicular/proconve/, last access: 1 April 2022, 2022.

Cheong, Y., Kim, T., Ryu, J. et al. Source apportionment of $PM_{2.5}$ using DN-PMF in three megacities in South Korea. Air Qual Atmos Health 17, 2579–2599. https://doi.org/10.1007/s11869-024-01584-5, 2024.

Chow, W. S., Liao, K., Huang, X. H. H., Leung, K. F., Lau, A. K. H. and Yu, J. Z.: Measurement report: The 10-year trend of $PM_{2.5}$ major components and source tracers from 2008 to 2017 in an urban site of Hong Kong, China, Atmospheric Chemistry and Physics, 22(17), 11557–11577, https://doi.org/10.5194/acp-22-11557-2022, 2022a.

Chow, W. S., Huang, X. H. H., Leung, K. F., Huang, L., Wu, X. and Yu, J. Z.: Molecular and elemental marker-based source apportionment of fine particulate matter at six sites in Hong Kong, China., Sci. Total Environ., 813, 152652, https://doi.org/10.1016/j.scitotenv.2021.152652, 2022b.

951  Clemente, Á., Yubero, E., Nicolás, J.F., Crespo, J. and Galindo N.: Organic tracers in fine and coarse aerosols at an urban
952  Mediterranean site: contribution of biomass burning and biogenic emissions. Environ Sci Pollut Res 31, 25216–25226
953  https://doi.org/10.1007/s11356-024-32789-x , 2024.

954  Cohen, A.J., Brauer, M., Burnett, R., Anderson, H.R., Frostad, J., Estep, K., Balakrishnan, K., Brunekreef, B., Dandona, L.,
955  Dandona, R., Feigin, V., Freedman, G., Hubbell, B., Jobling, A., Kan, H., Knibbs, L., Liu, Y., Martin, R., Morawska, L., Pope,
956  C.A. 3rd, Shin, H., Straif, K., Shaddick, G., Thomas, M., van Dingenen, R., van Donkelaar, A., Vos, T., Murray, C.J.L.,
957  Forouzanfar, M.H.: Estimates and 25-year trends of the global burden of disease attributable to ambient air pollution: an
958  analysis of data from the Global Burden of Diseases Study 2015, The Lancet, 389(10082), 1907–1918, 2017. Available at:
959  https://doi.org/10.1016/S0140-6736(17)30505-6.

960  La Colla, N. S., Botté, S.E., and Marcovecchio, J.E.: Atmospheric particulate pollution in South American megacities.,
961  Environ. Rev. 29, 3, https://doi.org/10.1139/er-2020-0105, 2021.

962  CONAMA: Conselho Nacional de MEio Ambiente - Resolução No. 491, 19 De Novembro de 2018,
963  http://www2.mma.gov.br/port/conama/legiabre.cfm?codlegi=740, last access: 12 December 2018, 2018.

964  Contini, D., Cesari, D., Conte, M. and Donateo, A.: Application of PMF and CMB receptor models for the evaluation of the
965  contribution of a large coal-fired power plant to $PM_{10}$ concentrations., Sci. Total Environ., 560–561, 131–140,
966  https://doi.org/10.1016/j.scitotenv.2016.04.031, 2016.

967  Dawidowski, L., Constantin, J.G., Murillo, J.H., Gómez-Marín, M., Nogueira, T., Jiménez, S.B., Díaz-Suárez, V., Victorica,
968  F.B., Lichtig, P., Resquin, M.D., Vargas-Rojas, M., Murillo-Hernández, J., Correa, J.A.V., Andrade, M.F., dos Santos, D.M.,
969  Maldonado, J.F., Aldape, F., Abreu, L.F., Manousakas, M.I. Carbonaceous fraction in $PM_{2.5}$ of six Latin American cities:
970  Seasonal variations, sources and secondary organic carbon contribution, Sci. Total Environ, 948, 174630,
971  https://doi.org/10.1016/j.scitotenv.2024.174630, 2024.

972  Decesari, S., Fuzzi, S., Facchini, M. C., Mircea, M., Emblico, L., Cavalli, F., Maenhaut, W., Chi, X., Schkolnik, G., Falkovich,
973  A., Rudich, Y., Claeys, M., Pashynska, V., Vas, G., Kourtchev, I., Vermeylen, R., Hoffer, A., Andreae, M. O., Tagliavini, E.,
974  Moretti, F. and Artaxo, P.: Characterization of the organic composition of aerosols from Rondônia, Brazil, during the LBA-
975  SMOCC 2002 experiment and its representation through model compounds, , https://doi.org/10.5194/acpd-5-5687-2005, 2005.

976  De La Torre-Roche, R. J., Lee, W.-Y. and Campos-Díaz, S. I.: Soil-borne polycyclic aromatic hydrocarbons in El Paso, Texas:
977  analysis of a potential problem in the United States/Mexico border region., J. Hazard. Mater., 163(2–3), 946–958,
978  https://doi.org/10.1016/j.jhazmat.2008.07.089, 2009.

979  Draxler, R. and Rolph, G.: HYSPLIT (Hybrid Single-Particle Lagrangian Integrated Trajectory) model, NOAA Air Resour.
980  Lab., Silver Spring, MD., 2003.

981  Emygdio, A.P.M., Andrade, M.F., Gonçalves, F.L.T., Engling, G., Zanetti, R.H.S., Kumar, P. Biomarkers as indicators of
982  fungal biomass in the atmosphere of São Paulo, Brazil. Sci. Total Environ., 612, 809-821,
983  https://doi.org/10.1016/j.scitotenv.2017.08.153, 2018.

984  Faisal, M., Ali, U., Kumar, A., Hazarika, N., Singh, V. and Kumar, M.: Festive fireworks in Delhi: A major source of elemental
985  aerosols established through dispersion normalized PMF in a multiyear study, Atmos. Environ., 323, 120394,
986  https://doi.org/10.1016/j.atmosenv.2024.120394, 2024.

987  Ferrari, C.P., Hong, S.,Van de Velde, K., Boutron, C.F., Rudniev, S.N., Bolshov, M., Chisholm, W., Rosman, K.J.R.: Natural
988  and anthropogenic bismuth in Central Greenland, Atmos. Environ., 34, 941-948, https://doi.org/10.1016/S1352-
989  2310(99)00257-5, 2000.

990  Ferreira da Silva, M., Vicente de Assunção, J., de Fátima Andrade, M. and Pesquero, C. R.: Characterization of metal and
991  trace element contents of particulate matter ($PM_{10}$) emitted by vehicles running on Brazilian fuels-hydrated ethanol and
992  gasoline with 22% of anhydrous ethanol., J. Toxicol. Environ. Health Part A, 73(13–14), 901–909,
993  https://doi.org/10.1080/15287391003744849, 2010.

994  Fine, P. M., Cass, G. R. and Simoneit, B. R.: Chemical characterization of fine particle emissions from fireplace combustion
995  of woods grown in the northeastern United States., Environ. Sci. Technol., 35(13), 2665–2675,
996  https://doi.org/10.1021/es001466k, 2001.

997  Fountoukis, C. and Nenes, A.: ISORROPIA II: a computationally efficient thermodynamic equilibrium model for $K^+$–$Ca^{2+}$–
998  $Mg^{2+}$–$NH_4^+$–$Na^+$–$SO_4^{2-}$–$NO_3^-$–$Cl^-$–$H_2O$ aerosols, Atmospheric Chemistry and Physics, 7(17), 4639–4659,
999  https://doi.org/10.5194/acp-7-4639-2007, 2007.

1000 Galvão, E.S., Reis, N.C., Lima, A.T., Stuetz, R.M., Orlando, M.T.A., Santos, J.M.: Use of inorganic and organic markers

1001  associated with their directionality for the apportionment of highly correlated sources of particulate matter, Sci. Total Environ.,
1002  651, 1332-1343, https://doi.org/10.1016/j.scitotenv.2018.09.263, 2019.Gioia, S. M. C. L., Babinski, M., Weiss, D. J., Spiro,
1003  B., Kerr, A. A. F. S., Veríssimo, T. G., Ruiz, I. and Prates, J. C. M.: An isotopic study of atmospheric lead in a megacity after
1004  phasing out of leaded gasoline, Atmos. Environ., 149, 70–83, https://doi.org/10.1016/j.atmosenv.2016.10.049, 2017.

1005  Gómez Peláez, L. M., Santos, J. M., de Almeida Albuquerque, T. T., Reis, N. C., Andreão, W. L. and de Fátima Andrade, M.:
1006  Air quality status and trends over large cities in South America, Environmental Science & Policy, 114, 422–435,
1007  https://doi.org/10.1016/j.envsci.2020.09.009, 2020.

1008  Gonçalves, C., Alves, C., Fernandes, A.P., Monteiro, C., Tarelho, L., Evtyugina, M., Pio, C.: Organic compounds in $PM_{2.5}$
1009  emitted from fireplace and woodstove combustion of typical Portuguese wood species, Atmos. Environ., 45, 4533-4545,
1010  https://doi.org/10.1016/j.atmosenv.2011.05.071, 2011.

1011  Gonçalves, C., Rienda, I.C., Pina, N., Gama, C., Nunes, T., Tchepel, O., Alves, C.: $PM_{10}$-Bound Sugars: Chemical
1012  Composition, Sources and Seasonal Variations. Atmosphere, 12, 194, https://doi.org/10.3390/atmos12020194, 2021.

1013  Goss, M., Swain, D.L., Abatzoglou, J.T., Sarhadi, A., Kolden, C.A., Williams, A.P., Diffenbaugh, N. S. Climate change is
1014  increasing the likelihood of extreme autumn wildfire conditions across California Environ. Res. Lett., 15, 9,
1015  https://doi.org/10.1088/1748-9326/ab83a7, 2020.

1016  Graham, B.: Water-soluble organic compounds in biomass burning aerosols over Amazonia1. Characterization by NMR and
1017  GC-MS, J. Geophys. Res., 107(D20), 8047, https://doi.org/10.1029/2001JD000336, 2002.

1018  Guo, S., Hu, M., Wang, Z. B., Slanina, J. and Zhao, Y. L.: Size-resolved aerosol water-soluble ionic compositions in the
1019  summer of Beijing: implication of regional secondary formation, Atmospheric Chemistry and Physics, 10(3), 947–959,
1020  https://doi.org/10.5194/acp-10-947-2010, 2010.

1021  Hall, D., Wu, C.-Y., Hsu, Y.-M., Stormer, J., Engling, G., Capeto, K., Wang, J., Brown, S., Li, H.-W. and Yu, K.-M.: PAHs,
1022  carbonyls, VOCs and $PM_{2.5}$ emission factors for pre-harvest burning of Florida sugarcane, Atmos. Environ., 55, 164–172,
1023  https://doi.org/10.1016/j.atmosenv.2012.03.034, 2012.

1024  Han, Y.-S, Eun, D.-M., Lee, G., Gong, S.Y., Youn, J.-S., Enhancement of $PM_{2.5}$ source appointment in a large industrial city
1025  of Korea by applying the elemental carbon tracer method for positive matrix factorization (PMF) model, Atmospheric Pollution
1026  Research, Volume 14, 101910,https://doi.org/10.1016/j.apr.2023.101910, 2023.

1027  Hetem, I.G., and Andrade, M.F.: Characterization of fine particulate matter emitted from the resuspension of road and
1028  pavement dust in the Metropolitan Area of São Paulo, Brazil, Atmos., 7, 31, https://doi.org/10.3390/atmos7030031, 2016.

1029  Huang, X., Liu, Z., Zhang, J., Wen, T., Ji, D. and Wang, Y.: Seasonal variation and secondary formation of size-segregated
1030  aerosol water-soluble inorganic ions during pollution episodes in Beijing, Atmos. Res., 168, 70–79,
1031  https://doi.org/10.1016/j.atmosres.2015.08.021, 2016.

1032  IAG-USP. Boletim Climatológico Anual da Estação Meteorológica do IAG/USP. Seção Técnica de Serviços Meteorológicos
1033  – Instituto de Astronomia, Geofísica e Ciências Atmosféricas da Universidade de São Paulo – vol. 22, 2019, São Paulo,
1034  IAG/USP, 2023

1035  Ianniello, A., Spataro, F., Esposito, G., Allegrini, I., Hu, M., and Zhu, T.: Chemical characteristics of inorganic ammonium
1036  salts in $PM_{2.5}$ in the atmosphere of Beijing (China), Atmos. Chem. Phys., 11(21), 10803–10822., https://doi.org/10.5194/acp-
1037  11-10803-2011, 2011.

1038  INPE: INPE (Instituto Nacional de Pesquisas Espaciais) – Portal do Monitoramento de Queimadas, available at:
1039  https://queimadas. dgi.inpe.br/queimadas/ (last access: 1 February 2024), 2019.

1040  Jang, H.-N., Seo, Y.-C., Lee, J.-H., Hwang, K.-W., Yoo, J.-I., Sok, C.-H. and Kim, S.-H.: Formation of fine particles enriched
1041  by V and Ni from heavy oil combustion: Anthropogenic sources and drop-tube furnace experiments, Atmos. Environ., 41(5),
1042  1053–1063, https://doi.org/10.1016/j.atmosenv.2006.09.011, 2007.

1043  Johnson, G. R., Juwono, A. M., Friend, A. J., Cheung, H.-C., Stelcer, E., Cohen, D., Ayoko, G. A. and Morawska, L.: Relating
1044  urban airborne particle concentrations to shipping using carbon based elemental emission ratios, Atmos. Environ., 95, 525–
1045  536, https://doi.org/10.1016/j.atmosenv.2014.07.003, 2014.

1046  Jung, J., Lee, S., Kim, H., Kim, D., Lee, H. and Oh, S.: Quantitative determination of the biomass-burning contribution to
1047  atmospheric carbonaceous aerosols in Daejeon, Korea, during the rice-harvest period, Atmos. Environ., 89, 642–650,
1048  https://doi.org/10.1016/j.atmosenv.2014.03.010, 2014.

Justo, E.P.S., Quijano, M.F.C., Beringui, K., Ventura, L.B., Pereira, G.M., Vasconcellos, P.C., Gioda, A.: Assessment of the impact of the bus fleet and transportation infrastructure works on the air quality in Rio de Janeiro (Olympic Games 2016). Air Qual. Atmos. Health., 16, 289–309, https://doi.org/10.1007/s11869-022-01275-z, 2023.Keyte, I.J., Harrison, R.M., and Lammel, G.: Chemical reactivity and long-range transport potential of polycyclic aromatic hydrocarbons – a review, Chem. Soc. Rev., 42, 9333-9391, https://doi.org/10.1039/C3CS60147A, 2013.

Khan, Z. Y., Kettler, J., Khwaja, H. A., Naqvi, I. I., Malik, A. and Stone, E. A.: Organic aerosol characterization and source identification in Karachi, Pakistan, Aerosol Air Qual. Res., 18(10), 2550–2564, https://doi.org/10.4209/aaqr.2017.12.0579, 2018.

Knorr, W., Dentener, F., Lamarque, J.-F., Jiang, L., Arneth, A., 2017. Wildfire air pollution hazard during the 21st century. Atmos. Chem. Phys. 17, 9223–9236. https://doi.org/10.5194/acp-17-9223-2017, 2017.

Kováts, N., Hubai, K., Sainnokhoi, T.-A., Hoffer, A. and Teke, G.: Ecotoxicity testing of airborne particulate matter-comparison of sample preparation techniques for the Vibrio fischeri assay., Environ. Geochem. Health, 43(11), 4367–4378, https://doi.org/10.1007/s10653-021-00927-w, 2021.

Kulkarni, P., Chellam, S. and Fraser, M. P.: Lanthanum and lanthanides in atmospheric fine particles and their apportionment to refinery and petrochemical operations in Houston, TX, Atmos. Environ., 40(3), 508–520, https://doi.org/10.1016/j.atmosenv.2005.09.063, 2006.

Kumar, P., de Fatima Andrade, M., Ynoue, R. Y., Fornaro, A., de Freitas, E. D., Martins, J., Martins, L. D., Albuquerque, T., Zhang, Y. and Morawska, L.: New directions: From biofuels to wood stoves: The modern and ancient air quality challenges in the megacity of São Paulo, Atmos. Environ., 140, 364–369, https://doi.org/10.1016/j.atmosenv.2016.05.059, 2016.

Kumar, S., Aggarwal, S. G., Gupta, P. K. and Kawamura, K.: Investigation of the tracers for plastic-enriched waste burning aerosols, Atmos. Environ., 108, 49–58, https://doi.org/10.1016/j.atmosenv.2015.02.066, 2015.

Kumar, P., Morawska, L., Birmili, W., Paasonen, P., Hu, M., Kulmala, M., Harrison, R. M., Norford, L., and Britter, R.: Ultra fine particles in cities, Environ. Int., 66, 1–10, https://doi.org/10.1016/j.envint.2014.01.013, 2014.

Lang, Y.-H., Li, G., Wang, X.-M., and Peng, P.: Combination of Unmix and PMF receptor model to apportion the potential sources and contributions of PAHs in wetland soils from Jiaozhou Bay, China, Mar. Pollut. Bull., 90, 129–134, https://doi.org/10.1016/j.marpolbul.2014.11.009, 2015

Lee, J. D.: Concise Inorganic Chemistry, 5th Edn., Willey, 1070 pp., 1999.

Lima, F.D.M. *Quantificação e caracterização físico-química do material particulado fino (MP2,5): queima de biomassa em fornos de pizzaria na cidade de São Paulo*. Master thesis - University of São Paulo, 2015.

Linak, W. P., Miller, C. A., Wood, J. P., Shinagawa, T., Yoo, J.-I., Santoianni, D. A., King, C. J., Wendt, J. O. L. and Seo, Y.-C.: High temperature interactions between residual oil ash and dispersed kaolinite powders, Aerosol Science and Technology, 38(9), 900–913, https://doi.org/10.1080/027868290500805, 2004.

Li, Q.-F., Wang-Li, L., Shah, S. B., Jayanty, R. K. M. and Bloomfield, P.: Ammonia concentrations and modeling of inorganic particulate matter in the vicinity of an egg production facility in Southeastern USA., Environ. Sci. Pollut. Res. Int., 21(6), 4675–4685, https://doi.org/10.1007/s11356-013-2417-z, 2014.

Li, W., Ge, P., Chen, M., Tang, J., Cao, M., Cui, Y., Hu, K. and Nie, D.: Tracers from Biomass Burning Emissions and Identification of Biomass Burning, Atmosphere, 12(11), 1401, https://doi.org/10.3390/atmos12111401, 2021.

Li, J., Carlson, B.E., Yung, Y.L., Lv, D., Hansen, J., Penner, J.E., Liao, H., Ramaswamy, V., Kahn, R.A., Zhang, P., Dubovik, O., Ding, A., Lacis, A.A., Zhang, L., Dong, Y.: Scattering and absorbing aerosols in the climate system. Nat. Rev. Earth Environ. 3, 363–379, https://doi.org/10.1038/s43017-022-00296-7, 2022.

Massimi, L., Simonetti, G., Buiarelli, F., Di Filippo, P., Pomata, D., Riccardi, C., Ristorini, M., Astolfi, M.L., Canepari, S.: Spatial distribution of levoglucosan and alternative biomass burning tracers in atmospheric aerosols, in an urban and industrial hot-spot of Central Italy, Atmos. Res., 239, 104904, https://doi.org/10.1016/j.atmosres.2020.104904, 2020.

Marynowski, L., and Simoneit, B.R.T.: Saccharides in atmospheric particulate and sedimentary organic matter: status overview and future perspectives, Chemosphere, 288, 132376, https://doi.org/10.1016/j.chemosphere.2021.132376, 2022.

Mbengue, S., Vodička, P., Komínková, K., Zíková, N., Schwarz, J., Prokeš, R., Suchánková, L., Julaha, K., Ondráček, J., Holoubek, I. and Ždímal, V.: Different approaches to explore the impact of COVID-19 lockdowns on carbonaceous aerosols at a European rural background site., Sci. Total Environ., 892, 164527, https://doi.org/10.1016/j.scitotenv.2023.164527, 2023.

Mehdi, Y., Hornick, J.-L., Istasse, L. and Dufrasne, I.: Selenium in the environment, metabolism and involvement in body functions., Molecules, 18(3), 3292–3311, https://doi.org/10.3390/molecules18033292, 2013.

Menares, C., Gallardo, L., Kanakidou, M., Seguel, R., Huneeus, N.: Increasing trends (2001–2018) in photochemical activity and secondary aerosols in Santiago, Chile. Tellus B: Chem. Phys. Meteorol., 72(1), 1–18. https://doi.org/10.1080/16000889.2020.1821512, 2020.

Meng, J., Li, Z., Zhou, R., Chen, M., Li, Y., Yi, Y., Ding, Z., Li, H., Yan, L., Hou, Z. and Wang, G.: Enhanced photochemical formation of secondary organic aerosols during the COVID-19 lockdown in Northern China., Sci. Total Environ., 758, 143709, https://doi.org/10.1016/j.scitotenv.2020.143709, 2021.

de Miranda, R.M., Lopes, F., do Rosário, N.É., Yamasoe, M.A., Landulfo, E., and Andrade, M.F.: The relationship between aerosol particles chemical composition and optical properties to identify the biomass burning contribution to fine particles concentration: a case study for São Paulo city, Brazil., Environ. Monit. Assess. 189, 6, https://doi.org/10.1007/s10661-016-5659-7, 2017.

MME, Ministério de Minas e Energia (Ministry of Mines and Energy - Brazil). National Agency of Petroleum, Natural Gas and Biofuels - Brazilian Statistical Yearbook of Petroleum, Natural Gas and Biofuels, 2023, available at: https://www.gov.br/anp/pt-br/centrais-de-conteudo/publicacoes/anuario-estatistico/arquivos-anuario-estatistico-2023/anuario-2023.pdf/view, (last access: 15 January 2024) 2023.

MME, Ministério de Minas e Energia (Ministry of Mines and Energy - Brazil). National Agency of Petroleum, Natural Gas and Biofuels - RESOLUÇÃO ANP Nº 968, DE 30 DE ABRIL DE 2024 (ANP RESOLUTION No. 968, OF APRIL 30, 2024) available at: https://www.in.gov.br/en/web/dou/-/resolucao-anp-n-968-de-30-de-abril-de-2024-557405632, (last access: 01 July 2024), 2024.

Monteiro dos Santos, D., Rizzo, L. V., Carbone, S., Schlag, P. and Artaxo, P.: Physical and chemical properties of urban aerosols in São Paulo, Brazil: links between composition and size distribution of submicron particles, Atmospheric Chemistry and Physics, 21(11), 8761–8773, https://doi.org/10.5194/acp-21-8761-2021, 2021.

Monteiro dos Santos, D. A., Brito, J. F., Godoy, J. M. and Artaxo, P.: Ambient concentrations and insights on organic and elemental carbon dynamics in São Paulo, Brazil, Atmos. Environ., 144, 226–233, https://doi.org/10.1016/j.atmosenv.2016.08.081, 2016.

Nava, S., Calzolai, G., Chiari, M., Giannoni, M., Giardi, F., Becagli, S., Severi, M., Traversi, R., Lucarelli, F.: Source Apportionment of $PM_{2.5}$ in Florence (Italy) by PMF Analysis of Aerosol Composition Records. Atmosphere, 11, 484. https://doi.org/10.3390/atmos11050484, 2020.

Norris, G., Duvall, R., Brown, S. and Bai, S.: EPA Positive Matrix Factorization (PMF) 5.0 Fundamentals and User Guide, 2014.

Oduber, F., Calvo, A. I., Castro, A., Alves, C., Blanco-Alegre, C., Fernández-González, D., Barata, J., Calzolai, G., Nava, S., Lucarelli, F., Nunes, T., Rodríguez, A., Vega-Maray, A. M., Valencia-Barrera, R. M. and Fraile, R.: One-year study of airborne sugar compounds: Cross-interpretation with other chemical species and meteorological conditions, Atmos. Res., 251, 105417, https://doi.org/10.1016/j.atmosres.2020.105417, 2021.

de Oliveira Alves, N., Brito, J., Caumo, S., Arana, A., de Souza Hacon, S., Artaxo, P., Hillamo, R., Teinilä, K., Batistuzzo de Medeiros, S. R. and de Castro Vasconcellos, P.: Biomass burning in the Amazon region: Aerosol source apportionment and associated health risk assessment, Atmos. Environ., 120, 277–285, https://doi.org/10.1016/j.atmosenv.2015.08.059, 2015.

de Oliveira Alves, N., Martins Pereira, G., Di Domenico, M., Costanzo, G., Benevenuto, S., de Oliveira Fonoff, A. M., de Souza Xavier Costa, N., Ribeiro Júnior, G., Satoru Kajitani, G., Cestari Moreno, N., Fotoran, W., Iannicelli Torres, J., de Andrade, J. B., Matera Veras, M., Artaxo, P., Menck, C. F. M., de Castro Vasconcellos, P., Saldiva, P.: Inflammation response, oxidative stress and DNA damage caused by urban air pollution exposure increase in the lack of DNA repair XPC protein, Environ. Int., 145,106150, https://doi.org/10.1016/j.envint.2020.106150, 2020.

Paatero, P. and Hopke, P. K.: Discarding or downweighting high-noise variables in factor analytic models, Anal. Chim. Acta, 490(1–2), 277–289, https://doi.org/10.1016/S0003-2670(02)01643-4, 2003.

Paatero, P. and Tapper, U.: Positive matrix factorization: A non-negative factor model with optimal utilization of error estimates of data values, Environmetrics, 5(2), 111–126, https://doi.org/10.1002/env.3170050203, 1994.

Pacheco, M. T., Parmigiani, M. M. M., de Fatima Andrade, M., Morawska, L. and Kumar, P.: A review of emissions and concentrations of particulate matter in the three major metropolitan areas of Brazil, J. Transp. Health, 4, 53–72, https://doi.org/10.1016/j.jth.2017.01.008, 2017.

1147 Parra, Y.J., Pereira, G.M., Custódio, D., de Figueiredo, S.B., Alves C., Vasconcellos P.C.: Aerosol characterization in a
1148 Central-West site of Brazil: influence of farming activities and toxicity. Air Qual Atmos Health 17, 599–620.
1149 https://doi.org/10.1007/s11869-023-01467-1, 2024.

1150 Pereira, P. A. de P., Lopes, W. A., Carvalho, L. S., da Rocha, G. O., Carvalho, N. De, Loyola, J., Quiterio, S. L., Escaleira, V.,
1151 Arbilla, G., and de Andrade, J. B.: Atmospheric concentrations and dry deposition fluxes of particulate trace metals in Salvador,
1152 Bahia, Brazil, Atmos. Environ., 41, 7837–7850, https://doi.org/10.1016/j.atmosenv.2007.06.013, 2007.

1153 Pereira, G. M., De Oliveira Alves, N., Caumo, S. E. S., Soares, S., Teinilä, K., Custódio, D., Hillamo, R., Alves, C. and
1154 Vasconcellos, P. C.: Chemical composition of aerosol in São Paulo, Brazil: influence of the transport of pollutants, Air Qual.
1155 Atmos. Health, 10(4), 457–468, https://doi.org/10.1007/s11869-016-0437-9, 2017a.

1156 Pereira, G. M., Teinilä, K., Custódio, D., Gomes Santos, A., Xian, H., Hillamo, R., Alves, C. A., Bittencourt de Andrade, J.,
1157 Olímpio da Rocha, G., Kumar, P., Balasubramanian, R., Andrade, M. de F. and de Castro Vasconcellos, P.: Particulate
1158 pollutants in the Brazilian city of São Paulo: 1-year investigation for the chemical composition and source apportionment,
1159 Atmospheric Chemistry and Physics, 17(19), 11943–11969, https://doi.org/10.5194/acp-17-11943-2017, 2017b.

1160 Pereira, G.M., Oraggio, B., Teinilä, K., Custódio, D., Huang, X., Hillamo, R., Alves, C.A., Balasubramanian, R., Rojas, N.Y.,
1161 Sanchez-Ccoyllo, O.R., and Vasconcellos, P.C.: A comparative chemical study of $PM_{10}$ in three Latin American cities: Lima,
1162 Medellín, and São Paulo. Air Qual. Atmos. Health, 12, 1141–1152, https://doi.org/10.1007/s11869-019-00735-3, 2019.

1163 Pereira, G. M., da Silva Caumo, S. E., Grandis, A., do Nascimento, E. Q. M., Correia, A. L., de Melo Jorge Barbosa, H.,
1164 Marcondes, M. A., Buckeridge, M. S. and de Castro Vasconcellos, P.: Physical and chemical characterization of the 2019
1165 "black rain" event in the Metropolitan Area of São Paulo, Brazil, Atmos. Environ., 248, 118229,
1166 https://doi.org/10.1016/j.atmosenv.2021.118229, 2021.

1167 Pereira, G. M., Kamigauti, L. Y., Nogueira, T., Gavidia-Calderón, M. E., Monteiro Dos Santos, D., Evtyugina, M., Alves, C.,
1168 Vasconcellos, P. de C., Freitas, E. D. and Andrade, M. de F.: Emission factors for a biofuel impacted fleet in South America's
1169 largest metropolitan area., Environ. Pollut., 331(Pt 2), 121826, https://doi.org/10.1016/j.envpol.2023.121826, 2023a.

1170 Pereira, G. M., Nogueira, T., Kamigauti, L. Y., Monteiro Dos Santos, D., Nascimento, E. Q. M., Martins, J. V., Vicente, A.,
1171 Artaxo, P., Alves, C., de Castro Vasconcellos, P. and de Fatima Andrade, M.: Particulate matter fingerprints in biofuel
1172 impacted tunnels in South America's largest metropolitan area., Sci. Total Environ., 856(Pt 2), 159006,
1173 https://doi.org/10.1016/j.scitotenv.2022.159006, 2023b.

1174 Pio, C. A., Legrand, M., Oliveira, T., Afonso, J., Santos, C., Caseiro, A., Fialho, P., Barata, F., Puxbaum, H., Sanchez-Ochoa,
1175 A., Kasper-Giebl, A., Gelencsér, A., Preunkert, S. and Schock, M.: Climatology of aerosol composition (organic versus
1176 inorganic) at nonurban sites on a west-east transect across Europe, J. Geophys. Res., 112(D23),
1177 https://doi.org/10.1029/2006JD008038, 2007.

1178 Pöschl, U.: Atmospheric aerosols: composition, transformation, climate and health effects., Angew. Chem. Int. Ed, 44(46),
1179 7520–7540, https://doi.org/10.1002/anie.200501122, 2005.

1180 Ravindra, K., Sokhi, R. and Vangrieken, R.: Atmospheric polycyclic aromatic hydrocarbons: Source attribution, emission
1181 factors and regulation, Atmos. Environ., 42(13), 2895–2921, https://doi.org/10.1016/j.atmosenv.2007.12.010, 2008.

1182 Ribeiro, F.N.D., de Oliveira, A.P., Soares, J., de Miranda, R.M., Barlage, M., Chen, F.: Effect of sea breeze propagation on
1183 the urban boundary layer of the metropolitan region of Sao Paulo, Brazil, Atmos. Res. 214, 174-188,
1184 https://doi.org/10.1016/j.atmosres.2018.07.015, 2018.

1185 da Rocha, G. O., Vasconcellos, P. de C., Ávila, S. G., Souza, D. Z., Reis, E. A. O., Oliveira, P. V., and Sanchez-Ccoyllo, O.:
1186 Seasonal distribution of airborne trace elements and water-soluble ions in São Paulo Megacity, Brazil, J. Braz. Chem. Soc.,
1187 23, 1915–1924, https://doi.org/10.1590/S0103-50532012005000062, 2012.

1188 Sánchez-Ccoyllo, O. R. and Andrade, M.F.: The influence of meteorological conditions on the behavior of pollutants
1189 concentrations in São Paulo, Brazil., Environ. Pollut., 116(2), 257–263, https://doi.org/10.1016/s0269-7491(01)00129-4, 2002.

1190 dos Santos, L.H.M., Kerr, A.A.F.S., Veríssimo, T.G., Andrade, M.F., de Miranda, R.M., Fornaro, A., and Saldiva, P.: Analysis
1191 of atmospheric aerosol ($PM_{2.5}$) in Recife city, Brazil. J. Air Waste Manag. Assoc., 64(5), 519–528.
1192 https://doi.org/10.1080/10962247.2013.854282, 2014.

1193 Santos, T. C. dos, Reboita, M. S. and Carvalho, V. S. B.: Investigação da Relação entre Variáveis Atmosféricas e a
1194 Concentração de $MP_{10}$ E $O_3$ no Estado de São Paulo, Rev. Bras. Meteorol., 33(4), 631–645, https://doi.org/10.1590/0102-
1195 7786334006, 2018.

Satsangi, A., Mangal, A., Agarwal, A., Lakhani, A., and Kumari, K. M.: Variation of carbonaceous aerosols and water soluble inorganic ions during winter haze in two consecutive years. Atmos. Pollut. Res., 12(3), 242–251, https://doi.org/10.1016/j.apr.2020.12.011, 2021.

Scaramboni, C. Impacto da queima de biomassa na concentração de compostos policíclicos aromáticos e na toxicidade *in vitro* do material particulado atmosférico de Ribeirão Preto-SP. Doctoral thesis - University of São Paulo, 2023.

Scaramboni, C., Farias,C.N., Vasconcellos, P.C., Levi, M., Sadiktsis, I., Pozza, S.A., Umbuzeiro, G.A., Watanabe, T., Rodrigues, P.C.O., Grandis, A., Pagliuso, D., Buckeridge, M.S., Campos, M.L.A.M., Kippler, M. Dreij, K., Galvão, M.F.O.: Characterization of cross-continental PM$_{2.5}$: Insights into emissions and chemical composition, Atmos. Res. 305, 107423, https://doi.org/10.1016/j.atmosres.2024.107423, 2024.

Schraufnagel, D. E.: The health effects of ultrafine particles., Exp. Mol. Med., 52(3), 311–317, https://doi.org/10.1038/s12276-020-0403-3, 2020.

SEADE, Fundação Sistema Estadual de Análise de Dados - São Paulo State Data Analysis System Foundation, available at: https://www.seade.gov.br/wp-content/uploads/2021/09/MapaIndustria_abril2019.pdf, (last access: 15 January 2024), 2019.

Serafeim, E., Besis, A., Kouras, A., Farias, C. N., Yera, A. B., Pereira, G. M., Samara, C. and de Castro Vasconcellos, P.: Oxidative potential of ambient PM$_{2.5}$ from São Paulo, Brazil: Variations, associations with chemical components and source apportionment, Atmos. Environ., 298, 119593, https://doi.org/10.1016/j.atmosenv.2023.119593, 2023.

Shen, H., Tao, S., Wang, R., Wang, B., Shen, G., Li, W., Su, S., Huang, Y., Wang, X., Liu, W., Li, B. and Sun, K.: Global time trends in PAH emissions from motor vehicles., Atmos. Environ., 45(12), https://doi.org/10.1016/j.atmosenv.2011.01.054, 2011.

Simoneit, B. R. T.: Biomass burning — a review of organic tracers for smoke from incomplete combustion, Applied Geochemistry, 17(3), 129–162, https://doi.org/10.1016/S0883-2927(01)00061-0, 2002.

Souto-Oliveira, C. E., Babinski, M., Araújo, D.F., and Andrade, M.F.: Multi-isotopic fingerprints (Pb, Zn, Cu) applied for urban aerosol source apportionment and discrimination, Sci. Total Environ., 626, 1350-1366, https://doi.org/10.1016/j.scitotenv.2018.01.192, 2018.

Souto-Oliveira, C. E., Kamigauti, L. Y., Andrade, M. F., and Babinski, M.: Improving Source Apportionment of Urban Aerosol Using Multi-Isotopic Fingerprints (MIF) and Positive Matrix Factorization (PMF): Cross-Validation and New Insights. Front. Environ. Sci. 9, 623915, https://doi.org/10.3389/fenvs.2021.623915,  2021.

Souto-Oliveira, C. E., Marques, M. T. A., Nogueira, T., Lopes, F. J. S., Medeiros, J. A. G., Medeiros, I. M. M. A., Moreira, G. A., da Silva Dias, P. L., Landulfo, E. and Andrade, M. de F.: Impact of extreme wildfires from the Brazilian Forests and sugarcane burning on the air quality of the biggest megacity on South America., Sci. Total Environ., 888, 163439, https://doi.org/10.1016/j.scitotenv.2023.163439, 2023.

Souza, D. Z., Vasconcellos, P. C., Lee, H., Aurela, M., Saarnio, K., Teinilä, K. and Hillamo, R.: Composition of PM$_{2.5}$ and PM$_{10}$ collected at urban sites in Brazil, Aerosol Air Qual. Res., 14(1), 168–176, https://doi.org/10.4209/aaqr.2013.03.0071, 2014.

Srivastava, D., Xu, J., Vu, T. V., Liu, D., Li, L., Fu, P., Hou, S., Moreno Palmerola, N., Shi, Z., and Harrison, R. M.: Insight into PM$_{2.5}$ sources by applying positive matrix factorization (PMF) at urban and rural sites of Beijing, Atmos. Chem. Phys., 21, 14703–14724, https://doi.org/10.5194/acp-21-14703-2021, 2021.

Sun, J., Shen, Z., Zhang, Y., Zhang, Q., Lei, Y., Huang, Y., Niu, X., Xu, H., Cao, J., Ho, S.S.H. and Li, X.: Characterization of PM$_{2.5}$ source profiles from typical biomass burning of maize straw, wheat straw, wood branch, and their processed products (briquette and charcoal) in China, Atmos. Environ. 205, 36-45, https://doi.org/10.1016/j.atmosenv.2019.02.038, 2019.

Tang, X., Zhang, X., Ci, Z., Guo, J. and Wang, J.: Speciation of the major inorganic salts in atmospheric aerosols of Beijing, China: Measurements and comparison with model, Atmos. Environ., 133, 123–134, https://doi.org/10.1016/j.atmosenv.2016.03.013, 2016.

Thorpe, A. and Harrison, R. M.: Sources and properties of non-exhaust particulate matter from road traffic: A review, Sci. Total Environ., 400(1–3), 270–282, https://doi.org/10.1016/j.scitotenv.2008.06.007, 2008.

Tobiszewski, M. and Namieśnik, J.: PAH diagnostic ratios for the identification of pollution emission sources., Environ. Pollut., 162, 110–119, https://doi.org/10.1016/j.envpol.2011.10.025, 2012.

Turpin, B.J., Lim, H.: Species contributions to PM$_{2.5}$ mass concentrations: revisiting common assumptions for estimating organic mass, Aerosol Sci. Technol., 35, 602-610, 2001.

Urban, R. C., Lima-Souza, M., Caetano-Silva, L., Queiroz, M. E. C., Nogueira, R. F. P., Allen, A. G., Cardoso, A. A., Held, G. and Campos, M. L. A. M.: Use of levoglucosan, potassium, and water-soluble organic carbon to characterize the origins of biomass-burning aerosols, Atmos. Environ., 61, 562–569, https://doi.org/10.1016/j.atmosenv.2012.07.082, 2012.

Urban, R. C., Alves, C. A., Allen, A. G., Cardoso, A. A., Queiroz, M. E. C. and Campos, M. L. A. M.: Sugar markers in aerosol particles from an agro-industrial region in Brazil, Atmos. Environ., 90, 106–112, https://doi.org/10.1016/j.atmosenv.2014.03.034, 2014.

Valente, F. and Laurini, M.: Pre-harvest sugarcane burning: A statistical analysis of the environmental impacts of a regulatory change in the energy sector, Cleaner Engineering and Technology, 4, 100255, https://doi.org/10.1016/j.clet.2021.100255, 2021.

Vara-Vela, A., Andrade, M. F., Kumar, P., Ynoue, R. Y. and Muñoz, A. G.: Impact of vehicular emissions on the formation of fine particles in the Sao Paulo Metropolitan Area: a numerical study with the WRF-Chem model, Atmospheric Chemistry and Physics, 16(2), 777–797, https://doi.org/10.5194/acp-16-777-2016, 2016.

Vasconcellos, P. C., Souza, D. Z., Sanchez-Ccoyllo, O., Bustillos, J. O. V, Lee, H., Santos, F. C., Nascimento, K. H., Araújo, M. P., Saarnio, K., Teinilä, K., and Hillamo, R.: Determination of anthropogenic and biogenic compounds on atmospheric aerosol collected in urban, biomass burning and forest areas in São Paulo, Brazil, Sci. Total Environ., 408, 5836–5844, https://doi.org/10.1016/j.scitotenv.2010.08.012, 2010.

Vieira-Filho, M. S., Ito, D. T., Pedrotti, J. J., Coelho, L. H. G. and Fornaro, A.: Gas-phase ammonia and water-soluble ions in particulate matter analysis in an urban vehicular tunnel., Environ. Sci. Pollut. Res. Int., 23(19), 19876–19886, https://doi.org/10.1007/s11356-016-7177-0, 2016a.

Vieira-Filho, M.S., Pedrotti, J. J., and Fornaro, A.: Water-soluble ions species of size-resolved aerosols: Implications for the atmospheric acidity in São Paulo megacity, Brazil, Atmos. Res., 181, 281–287, https://doi.org/10.1016/j.atmosres.2016.07.006, 2016b.

Vieira, E. V. R., do Rosario, N. E., Yamasoe, M. A., Morais, F. G., Martinez, P. J. P., Landulfo, E. and Maura de Miranda, R.: Chemical characterization and optical properties of the aerosol in São Paulo, Brazil, Atmosphere, 14(9), 1460, https://doi.org/10.3390/atmos14091460, 2023.

Watson, J.G., Chow, J.C., Houck, J.E.: PM$_{2.5}$ chemical source profiles for vehicle exhaust, vegetative burning, geological material, and coal burning in Northwestern Colorado during 1995, Chemosphere, 43, 1141-1151, https://doi.org/10.1016/S0045-6535(00)00171-5, 2001.

Wang Q.Q., L.P. Qiao, M. Zhou, S.H. Zhu, S. Griffith, L. Li, Yu. J.Z.: Source Apportionment of PM$_{2.5}$ Using Hourly Measurements of Elemental Tracers and Major Constituents in an Urban Environment: investigation of Time-Resolution Influence J. Geophys. Res.-Atmos., 123, 5284-5300, https://doi.org/10.1029/2017JD027877, 2018.

WHO, World Health Organization: WHO global air quality guidelines: Particulate matter (PM$_{2.5}$ and PM$_{10}$), ozone, nitrogen dioxide, sulfur dioxide and carbon monoxide, Geneva., 2021.

Wu, X., Vu, T. V., Shi, Z., Harrison, R. M., Liu, D. and Cen, K.: Characterization and source apportionment of carbonaceous PM$_{2.5}$ particles in China - A review, Atmos. Environ., 189, 187–212, https://doi.org/10.1016/j.atmosenv.2018.06.025, 2018.

Yamagami, M., Ikemori, F., Nakashima, H., Hisatsune, K. and Osada, K.: Decreasing trend of elemental carbon concentration with changes in major sources at Mega city Nagoya, Central Japan, Atmos. Environ., 199, 155–163, https://doi.org/10.1016/j.atmosenv.2018.11.014, 2019.

Yassaa, N., Meklati, B.Y., Cecinato, A., and Marino, F.: Organic aerosols in urban and waste landfill of Algiers metropolitan area: occurrence and sources, Environ. Sci. Technol. 35, 306–311, https://doi.org/10.1021/es991316d, 2001.

Yunker, M. B., Macdonald, R. W., Vingarzan, R., Mitchell, R. H., Goyette, D. and Sylvestre, S.: PAHs in the Fraser River basin: a critical appraisal of PAH ratios as indicators of PAH source and composition, Org. Geochem., 33(4), 489–515, https://doi.org/10.1016/S0146-6380(02)00002-5, 2002.

Yu, J. Z., Xu, J. and Yang, H.: Charring characteristics of atmospheric organic particulate matter in thermal analysis., Environ. Sci. Technol., 36(4), 754–761, https://doi.org/10.1021/es015540q, 2002.

Yuan, H., Zhuang, G., Li, J., Wang, Z., Li, J.: Mixing of mineral with pollution aerosols in dust season in Beijing: Revealed by source apportionment study, Atmo. Environ. 42, 2141-2157, ISSN 1352-2310, https://doi.org/10.1016/j.atmosenv.2007.11.048, 2008.

Zhang, W., Zhang, S., Wan, C., Yue, D., Ye, Y. and Wang, X.: Source diagnostics of polycyclic aromatic hydrocarbons in

urban road runoff, dust, rain and canopy throughfall., Environ. Pollut., 153(3), 594–601, https://doi.org/10.1016/j.envpol.2007.09.004, 2008.

Zhu, C.-S., Cao, J.-J., Tsai, C.-J., Shen, Z.-X., Han, Y.-M., Liu, S.-X. and Zhao, Z.-Z.: Comparison and implications of $PM_{2.5}$ carbon fractions in different environments., Sci. Total Environ., 466–467, 203–209, https://doi.org/10.1016/j.scitotenv.2013.07.029, 2014.

Zhu, C., Kawamura, K. and Kunwar, B.: Effect of biomass burning over the western North Pacific Rim: wintertime maxima of anhydrosugars in ambient aerosols from Okinawa, Atmospheric Chemistry and Physics, 15(4), 1959–1973, https://doi.org/10.5194/acp-15-1959-2015, 2015.